PERGAMON

Journal of Structural Geology 25 (2003) 351–370

JOURNAL OF STRUCTURAL GEOLOGY

www.elsevier.com/locate/jsg

Three-dimensional deformation along the rupture trace of the September 21st, 1999, Taiwan earthquake: a case study in the Kuangfu school

Jacques Angelier[a,*], Jian-Cheng Lee[b], Jyr-Ching Hu[c], Hao-Tsu Chu[d]

[a]*Séismotectonique et Tectonophysique, ESA 7072, Université Pierre et Marie Curie, Boîte 129, 4 place Jussieu, F-75252, Paris Cedex 05, France*
[b]*Institute of Earth Sciences, Academia Sinica, PO Box 1-55, Nankang, Taipei, Taiwan, ROC*
[c]*Institute for Secondary School Teachers of Taiwan, Fengyuan, Taichung, Taiwan, ROC*
[d]*Central Geological Survey, PO Box 968, Taipei, Taiwan, ROC*

Received 20 May 2001; accepted 5 May 2002

Abstract

In Central Taiwan, the destructive Chichi earthquake ($M_w = 7.6$) of September 21st, 1999, produced a nearly 100-km-long rupture trace following the Chelungpu Fault. This paper shows how the geometry of the fault slip can locally be determined in three dimensions, based on analyses of earthquake fault in the Kuangfu stadium. The fault at this site is reverse and left-lateral. The three-dimensional geometrical analysis, done with a variety of data through independent determination modes, all applied to the deformation of the surface layer of the stadium tracks, allows complete verification of the results. Not only do these analyses constrain the fault behaviour in terms of trend, dip angle, obliquity and amount of slip, but also they reveal variations in both the horizontal and the vertical fault geometry. The comparison with relative displacements recorded at larger distances from the fault reveals that slip partitioning occurs, with nearly dip-slip thrusting along the rupture trace and distributed left-lateral shear in a deformed zone of the hanging wall, adjacent to the main fault.

Keywords: Earthquake; Rupture trace; Surface fault; Fault slip; Taiwan

1. Introduction

A large destructive earthquake, the Chichi earthquake, occurred in central western Taiwan on September 21st, 1999 (Fig. 1a and b). More than 2400 inhabitants were killed while thousands of buildings were destroyed or damaged. The energy and local magnitudes ($M_W = 7.6$ and $M_L = 7.3$) indicated that it was the largest earthquake in Taiwan since the beginning of the twentieth century. The epicenter was located at 25°50.2′N and 121°49.5′E, 30 km SE of Taichung, the third largest city in the country (Central Weather Bureau of Taiwan, 1999; Institute of Earth Sciences, Academia Sinica, 1999). The focus was situated at a depth of about 5–12 km (Chung and Shin, 1999; Kao and Chen, 2000). Both the seismological records and the GPS measurements indicated co-seismic slip varying from a few metres to nearly 10 m (Ma et al., 1999; Hou et al., 2000). The earthquake source study for the main shock revealed thrust faulting along a plane dipping 25°E down to at least 15 km depth (Kao and Chen, 2000). Many aftershocks, with local magnitudes as large as 6.8, occurred during the following months. Based on stress tensor inversion of 115 events, Kao and Angelier (2001a,b) showed that the mechanisms of the Chichi sequence indicate a N119°E-trending regional compression, in agreement with the direction of relative motion between the Philippine Sea plate and Eurasia.

The 1999 Chichi earthquake produced a nearly continuous line of surface ruptures extending from north to south over a distance of nearly 100 km (Fig. 1b and c). The fault trace was mapped soon after the earthquake (Central Geological Survey, 1999a,b). The earthquake motion on this fault was of thrust type, with a left-lateral component. The longest segment of this fault trace corresponds to the N–S-trending Chelungpu Fault, a major geological and the morphological boundary between the Mio–Pliocene formations of the Foothills mountains to the east and the Plio–Quaternary basins, tablelands and coastal plain to the west (Fig. 1c). This region of central western Taiwan had been geologically mapped prior to the earthquake (Chinese Petroleum Corporation, 1974, 1982). The Taiwan mountain belt is interpreted as a result of the Plio–Pleistocene oblique collision between the Philippine Sea and Eurasian plates

* Corresponding author. Fax: +33-1-44-27-50-85.
E-mail address: jacques.angelier@lgs.jussieu.fr (J. Angelier).

0191-8141/03/$ - see front matter © 2002 Elsevier Science Ltd. All rights reserved.
PII: S0191-8141(02)00039-1

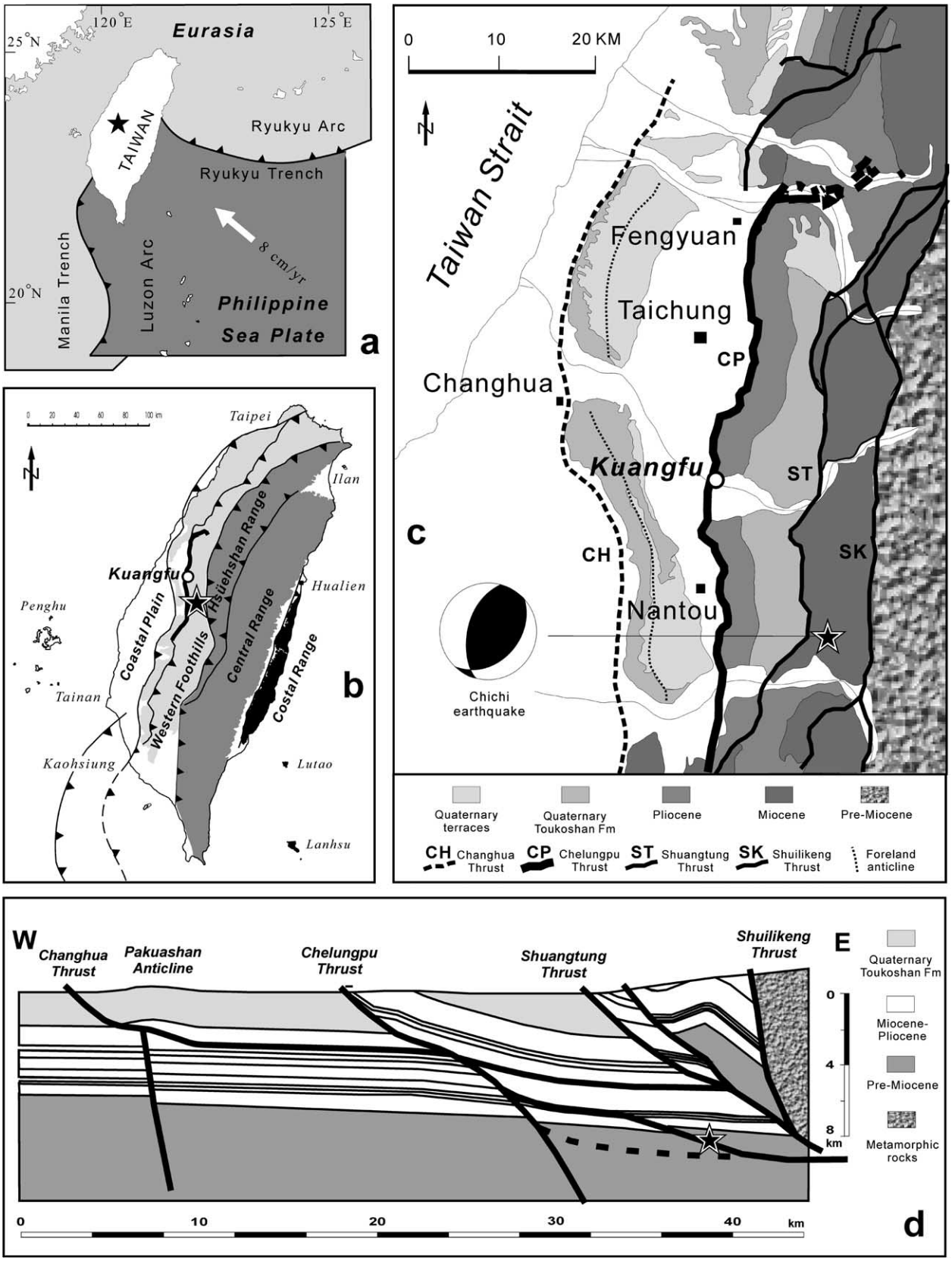

Fig. 1. Geological setting of studied area. Epicentre of Chichi earthquake (September 21st, 1999) as framed star in all sub-figures. (a) Plate tectonic framework, with Philippine Sea Plate in dark grey and triangles on upthrust side along subduction boundaries. (b) Main units of the Taiwan mountain belt, with major thrusts as lines with triangles on upthrust side and rupture trace of Chichi earthquake as thicker line. Kuangfu site as open dot. (c) Geological map of Chichi earthquake area. Stereoplot of mainshock focal mechanism (equal-area projection of lower hemisphere, compressive quadrants white). All thrusts are west-vergent. Kuangfu site as open dot. (d) Balanced cross-section near Taichung, modified after Mouthereau et al. (2001b).

(Ho, 1975, 1986; Suppe, 1976, 1981; Wu, 1978; Angelier, 1986; Tsai, 1986). The Chelungpu Fault is one of the largest west-verging thrusts near the front of this mountain belt (Fig. 1b).

The regional description of the surface ruptures associated with the 1999 Chichi earthquake is beyond the scope of this paper. Regional analyses of the generally N–S-trending rupture trace of the Chichi earthquake have been presented elsewhere (e.g. Angelier et al., 2001; Lee et al., 2001). Thrust scarps with vertical offsets in the range 2–6 m were observed along the fault. The co-seismic displacement generally increased from south to north. A specific structural study was devoted to the WNW–ESE-trending northern ruptures, where the vertical offset was largest, up to 8–10 m in some cases (Lee et al., 2001). The fault geometry at depth has been investigated through a comparison between seismological and geological data (Mouthereau et al., 2001a) as well as an inversion from GPS co-seismic measurements (Johnson et al., 2001). Balanced cross-sections (Fig. 1d) suggested that the location and mechanism of the Chichi earthquake were consistent with thrusting on a low-angle ramp connected at depth with a major detachment in the upper crust (Mouthereau et al., 2001b).

We carried out field investigation along the Chelungpu Fault during the first days following the Chichi earthquake. We aimed at identifying the structural characteristics of the surface ruptures that reveal the kinematics of faulting. We paid special attention to determine the displacement of the

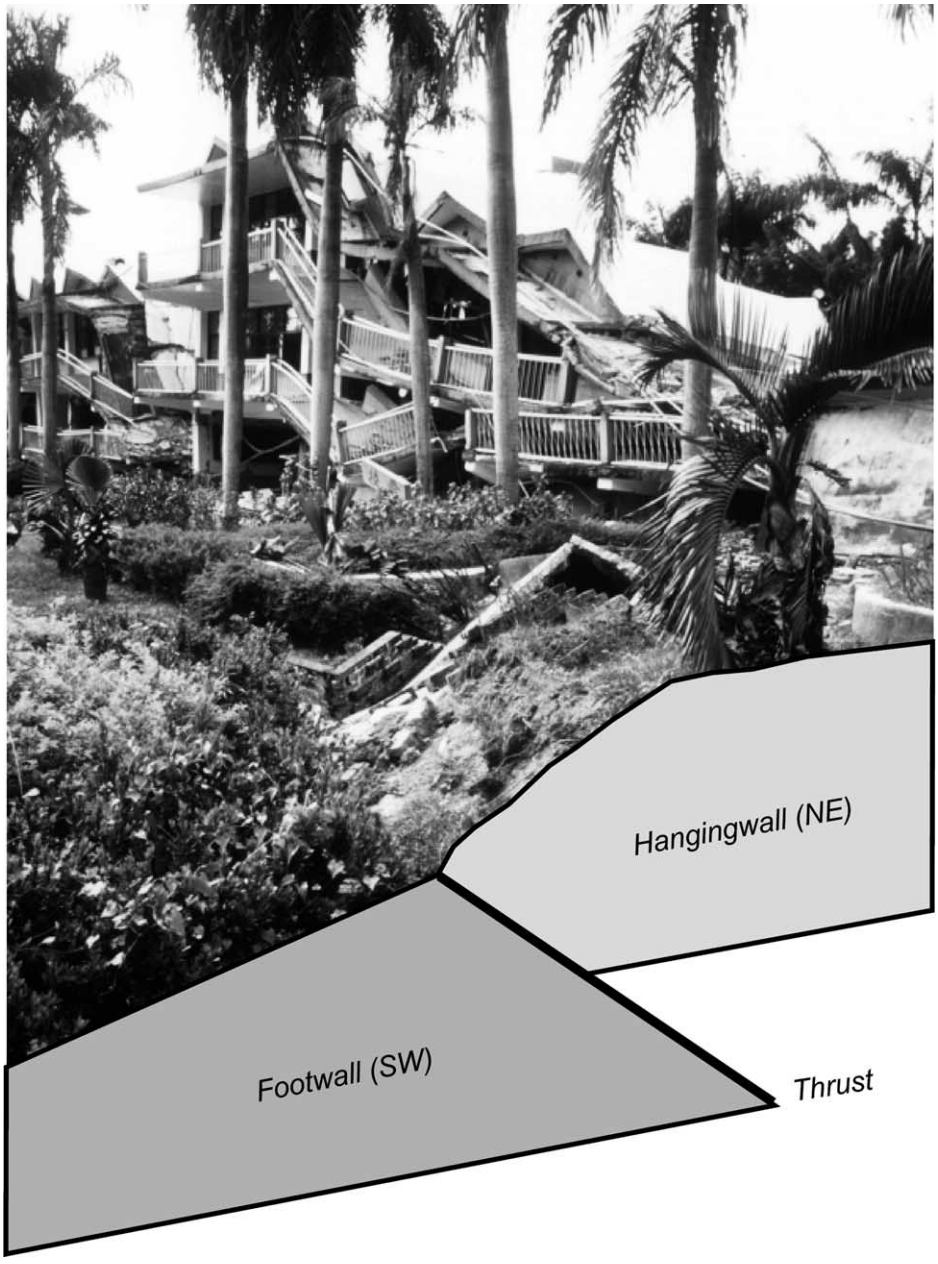

Fig. 2. The collapsed Kuangfu school. View towards the NW. Foreground: fault scarp of the September 21st earthquake, 1999.

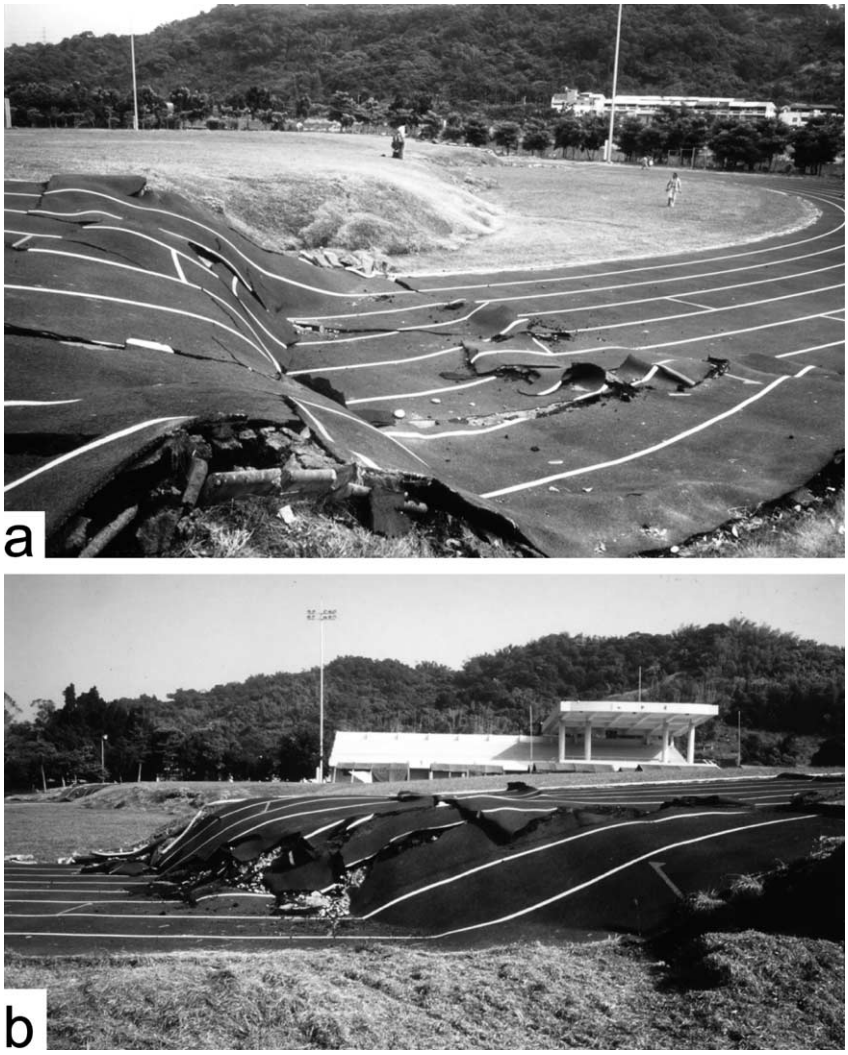

Fig. 3. The fault scarp of the September 21st earthquake, 1999, across the Kuangfu school stadium. Views towards SE (a) and N (b). Faulted stadium tracks at sub-sites A (a) and B (b), located in Fig. 4.

earthquake thrust fault in three dimensions. The surface ruptures that developed in the Kuangfu school, located in Fig. 1c (latitude 24°2.617′N, longitude 120°41.486′E), allow such a quantitative study. When the school buildings collapsed during the main shock (Fig. 2), no pupil was inside because the earthquake occurred during the night.

The aim of this paper is two-fold. On one hand, we reconstruct the co-seismic thrust deformation in a site where the rupture trace of the Chelungpu Fault is well exposed, within the frame of the Taiwan active collision. This site is certainly not ideal to analyse the regional behaviour of the rupture trace, because it is situated in a sharp bend of the shallow fault. This local bend, which is too small to be discernible at the scale of the map of Fig. 1c, has been mapped in detail by the Central Geological Survey (1999a). The local strike of the rupture trace, NW–SE over a distance of about 1 km, cannot be regarded as typical of the Chelungpu Fault, which strikes N–S at the regional scale (Fig. 1c). As a consequence of this particular situation, the slip geometry at Kuangfu should be interpreted with caution as far as the general behaviour of the earthquake fault is concerned. With respect to this, a more typical situation is analysed in another site farther to the north along the same fault trace (Angelier et al., 2002).

The site of the Kuangfu school, however, is ideal to carry out a complete methodological evaluation of the fault slip reconstruction techniques, because a variety of benchmarks enables one to determine the three-dimensional fault slip geometry in several ways, and hence to compare the results. We consequently carried out a detailed structural analysis in this site, in order to discuss the geometrical rules and evaluate their limitations. The main target of this paper is to evaluate the reliability and accuracy of the determination of fault behaviour indicated by surface deformation data.

To this respect, we took advantage of the presence at Kuangfu of a sport field cut and offset by the earthquake rupture (Fig. 3). Both the regular elliptical shape of the stadium tracks and the nature of their surface layer allowed

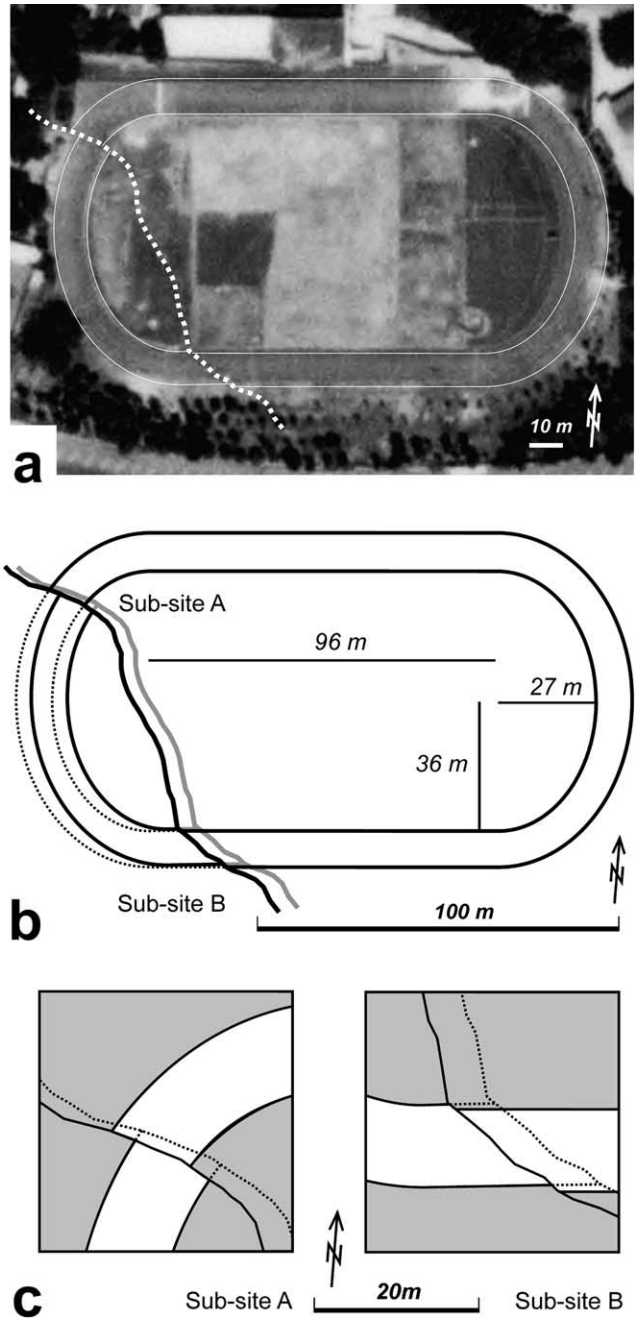

Fig. 4. Fault trace of the September 21st earthquake, 1999, across the Kuangfu stadium. (a) Aerial view of the stadium, with rupture trace as white dotted line. (b) Corresponding map of fault trace and location of sub-sites. (c) Maps of sub-sites, with stadium tracks left white and grassy areas in grey. Inferred approximate position of the buried footwall edge as dotted lines.

complete determination of the co-seismic fault displacement. Such artificial surface layers offer excellent potential for recording evidence of non-tectonic deformation (Roberts, 2000) as well as co-seismic faulting (Angelier and Bergerat, 2001). Not only did we choose the Kuangfu site as an example of the surface faulting of the 1999 Taiwan earthquake, but we could also check in detail the validity and accuracy of the geometrical methods. Particular attention was paid to uncertainties, based on consideration of both the technical measurement processes and the redundancy of several determinations carried out independently. In this paper, we thus explore some methodological aspects of the three-dimensional analysis using surface rupture data to determine the behaviour of a major earthquake fault. We finally compare the results with the regional co-seismic deformation indicated by the geodetic networks.

2. The fault scarp geometry in the Kuangfu stadium

The segment of the Chelungpu fault scarp across the Kuangfu stadium is about 100 m long and trends NW–SE (Fig. 4a and b). It is composed of three sub-segments. To the NW, at sub-site A (Fig. 3a), the scarp cuts across the western half-ellipse of the stadium (Fig. 4c). This sub-segment is 12 m long and strikes N125–130°E, almost perpendicular to the stadium tracks. Because of their elliptical shape, the tracks trend approximately N40°E on the hanging wall and N20° on the footwall. To the SE, at sub-site B (Fig. 3b), the scarp cuts across the southern straight line of the stadium (Fig. 4c). This sub-segment is 18 m long and strikes N125–135°E, oblique at an angle of about 45° to the tracks, which are rectilinear and trend N86°E on both sides of the rupture zone. Between A and B, the scarp runs across the central pool of the stadium; it is approximately 70 m long and strikes N152°E on average. The local fault strikes vary (Fig. 4b) because the shape of the scarp at sub-sites A and B was influenced by the mechanical response of the surface layers, including the stadium track cover. These local strikes do not reflect the fault geometry at depth, even at the 100-m-scale considered in our study. As a consequence, the average trend of the whole fault segment of the Kuangfu stadium, N141°E, is considered as the fault strike throughout this paper.

In order to determine the geometry of the fault scarp, measurements were performed along two N18°E trending profiles at sub-site A, and one N81°E-trending profile at sub-site B (Fig. 5). At the time of our field survey, in the first days after the Chichi earthquake, high-precision geodetic equipment was not available in this area. We consequently used a metric tape to determine the lengths, a compass to determine the azimuths, and a clinometer to determine the dip angles. Along each of the three profiles, we measured the length and the dip angle of 10–30 nearly rectilinear segments. The measurement accuracy was ± 0.001 m for lengths and about $\pm 0.5°$ for angles. The vertical and horizontal distances were obtained by multiplying each segment length by the sine and cosine of the dip angle, respectively. Most surfaces measured were nearly horizontal. As a consequence, the uncertainties remained small for horizontal distances but reached large values for vertical ones despite survey redundancy. Taking as an example a 1-m-long, nearly horizontal segment, the vertical uncertainty was as large as ± 0.01 m, ten times the horizontal one. The main

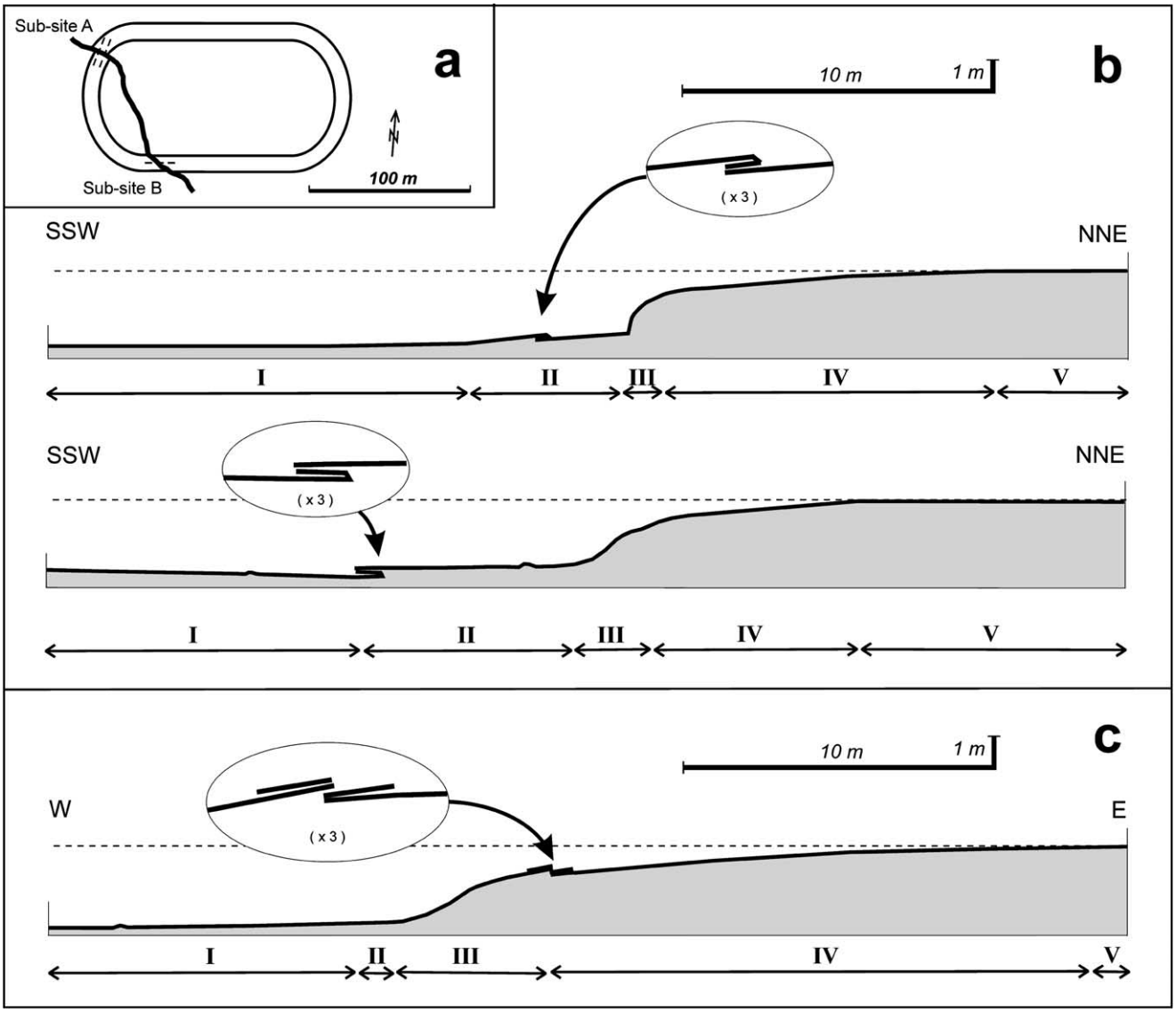

Fig. 5. Profiles of the fault scarp of the September 21st earthquake, 1999, in the Kuangfu stadium. (a) Location map, with profiles as thin dashed lines. (b) N18°E trending profiles at sub-site A. (c) N81°E trending profile at sub-site B. Below each profile, main units across rupture zone indicated by roman numbers: I: flat footwall domain; II: footwall with deformed synthetic cover; III: fault scarp; IV: flexure zone in hanging wall; V: flat hanging wall domain.

uncertainties in horizontal distances came from the observation, not from the measurement process. They were as large as ±0.02 m at some locations, especially where the cover is tightly folded (Fig. 3).

We estimated first the vertical offset, taking advantage of the initially horizontal surface of the stadium tracks on both sides of the rupture zone. We obtained total values of 2.43 ± 0.18 m on average at sub-site A and 2.87 ± 0.22 m

Table 1
Main determinations of fault slip geometry in the Kuangfu stadium. A–B, from shortening values at both sub-sites; B, from two components of displacement at sub-site B; A_1 and A_2, from the shift between elliptical stadium tracks at sub-site A (translation and translation–rotation, respectively). Lengths in metres, angles in degrees. *V*, vertical relative displacement; *T*, transverse horizontal slip; *L*, transverse lateral slip; dip, calculated dip angle of fault (to the NE); pitch, calculated pitch of slip vector in fault plane (to the SE); ω, azimuth of slip vector (footwall relative to hanging wall); *X*, horizontal component of slip

Sub-sites	*V*	*T*	*L*	Dip	Pitch	ω	*X*
A–B	2.65 ± 0.20	2.62 ± 0.19	0.52 ± 0.30	45 ± 4	82 ± 5	62 ± 7	2.67 ± 0.25
B	2.87 ± 0.22	2.61 ± 0.21	0.55 ± 0.18	48 ± 4	82 ± 3	63 ± 5	2.67 ± 0.24
A_1	2.43 ± 0.18	2.85 ± 1.04	1.78 ± 1.10	40 ± 13	65 ± 19	83 ± 14	3.36 ± 0.71
A_2	2.43 ± 0.18	2.33 ± 0.99	2.03 ± 1.02	46 ± 14	59 ± 18	92 ± 16	3.09 ± 0.60

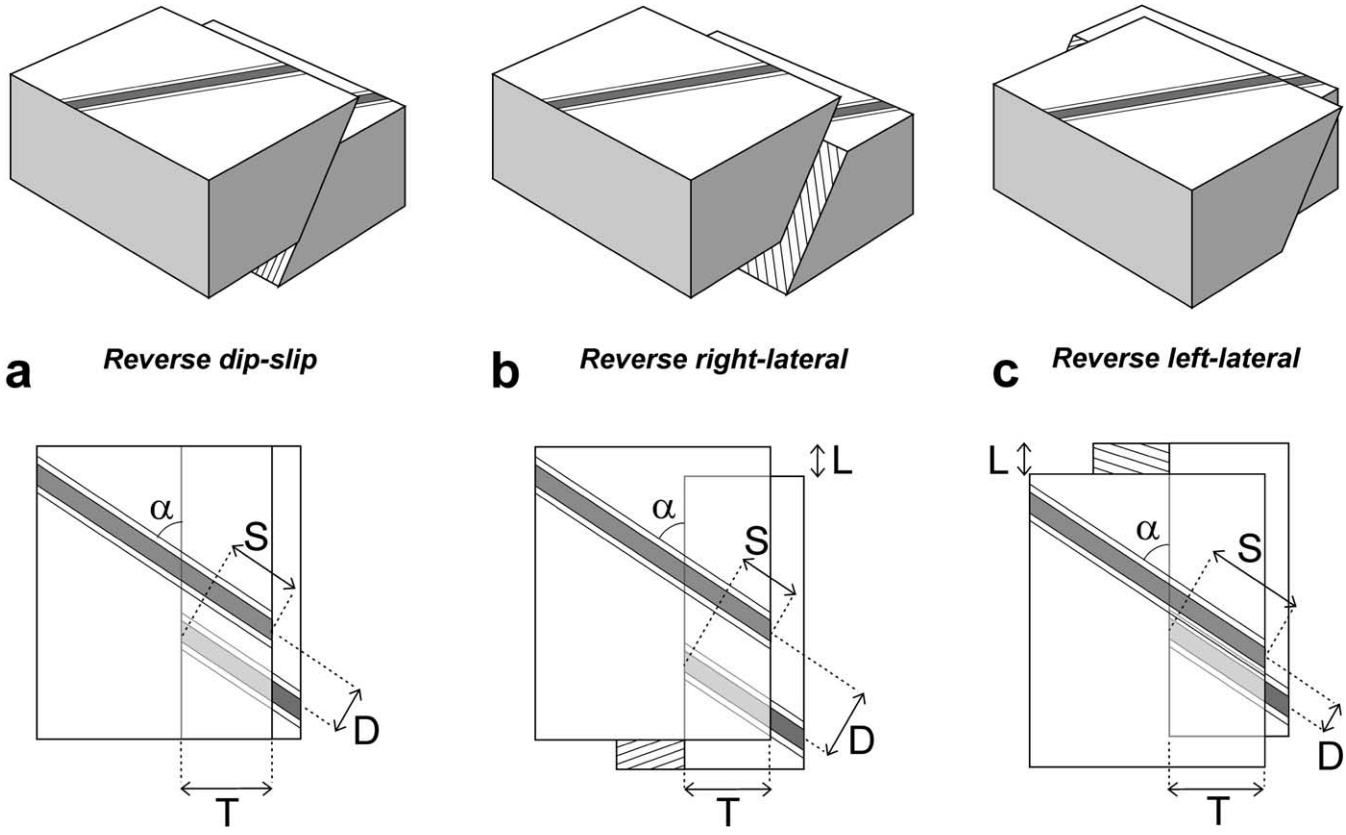

Fig. 6. Relationships between fault slip geometry and deformation of horizontal linear benchmarks. Situations of reverse dip-slip (a), reverse right-lateral (b) and reverse left-lateral (c) relative displacement. In map views: in light grey, portion of footwall block surface hidden by hanging wall; slip direction shown by striations on visible portion of fault. Angle between fault strike and linear benchmark as α, transverse horizontal fault relative displacement as T, lateral displacement as L. Amount of shortening of linear benchmark as S, strike-perpendicular horizontal offset of linear benchmark as D.

at sub-site B (Table 1). The tip zones of the profiles correspond to flat, non-deformed footwall and hanging wall domains (roman numbers I and V, respectively, in Fig. 5). In the scarp zone, each profile is composed of three main portions (roman numbers II, III and IV, from footwall to hanging wall, in Fig. 5). The central portion, 2–6 m long, reveals the shape of the scarp *stricto sensu*. The other two portions reveal the behaviour of the footwall- and hanging-wall-deformed edge zones. In the footwall portions of the profiles, the differences in elevation were small (about 0.35 and 0.17 m at sub-sites A and B, respectively). This indicates that very little near-fault tilting occurred in the footwall. In contrast, the hanging wall portions showed smooth but significant deformation, with differences in elevation as large as 0.65 and 0.96 m for sub-sites A and B, respectively. This shows that within distances of 10 and 20 m to the fault the hanging wall was deformed and tilted about 2–3° towards the footwall.

As the vertical sections of Fig. 5 show, the vertical offset measured across the 2–6-m-wide rupture trace is about 1.6–1.8 m at both sub-sites (A and B). This is roughly 1 m less than the total vertical offset, which includes the contribution of flexing and tilting within distances of 10–20 m on both sides of the rupture zone. We aim at quantifying the displacement of the earthquake fault (Fig. 4), so that the deformation near block edges must be integrated in the determination. As a consequence, the values considered in the subsequent calculations are the total vertical offsets determined in the profiles, not the height of the narrow fault scarp.

The amount of shortening along each of the three profiles could be reliably determined because of the behaviour of the synthetic surface layer used to build the stadium tracks. This layer, generally 0.10–0.15 m thick, deformed in a complex but consistent way so that at several places its general continuity was maintained (Fig. 3). Its response to the fault motion was complex and involved minor folding and thrusting. Open fissures and tear fractures accommodated variations in deformation, like transfer faults, between the opposite-verging folds in the footwall at sub-site A (Fig. 5). We reconstructed the deformation of this synthetic surface layer along straight survey lines. We ignored the survey lines where local disruption or destruction of the layer precluded continuous data collection.

For each profile, the amount of shortening was simply given by the comparison between the horizontal length of the profile and the total length of the deformed synthetic cover (that is, the original profile length). It was thus necessary to carefully measure the tight folds or small thrusts that developed at some places inside the layer (Fig. 5b and c).

The tips of each profile were fixed far enough from the rupture trace to include the whole deformation of the rupture zone. The two N18°E-trending profiles at sub-site A were 18.38 and 23.20 m long. The corresponding lengths of the deformed layer were 20.32 and 25.10 m. The resulting shortenings values, 1.94 and 1.90 m, respectively, are almost identical. The N81°E profile at sub-site B was 40.05 m long. The length of the deformed layer was 42.58 m, indicating a larger shortening value, 2.53 m. Considering the uncertainties, the profile-parallel shortening is 1.92 ± 0.14 m at sub-site A and 2.53 ± 0.18 m at sub-site B.

Not surprisingly, the main contribution to shortening comes from the central portion of each profile, the scarp itself. However, at sub-site A, opposite-verging tight folds developed in the surface layer at distances of about 3–6 m from the base of the scarp (Figs. 3a and 5b). They resulted in a local shortening of 0.9–1.4 m. Such folds formed because the surface layer pushed by the fault could slip, part of its shortening being transferred in the footwall. A similar phenomenon occurred in the hanging wall at sub-site B (Fig. 5c). These features, and the related shortening, should be attributed to motion in the scarp zone.

3. Comparison between shortenings as a key to fault slip (two sub-sites)

Before any exploitation of the results obtained at sub-sites A and B, it is necessary to keep in mind that the profiles are not fault-perpendicular, and that they are not parallel. Let us consider first a dip-slip fault with a transverse horizontal displacement, T (Fig. 6a). T is the fault-perpendicular horizontal shortening. The apparent shortening, S, of a rectilinear feature oblique at an angle α to the direction of the dip-slip fault is given by:

$$S = T\sin\alpha \quad (1)$$

At the scale considered in this study, the strike of the fault is N141°E (Fig. 4b), giving for α a value of 57° clockwise at sub-site A and 60° anticlockwise at sub-site B. Eq. (1) yields values of 2.29 ± 0.17 m at sub-site A and 2.92 ± 0.21 m at sub-site B, for the transverse component, T, of a dip-slip fault. The difference is large enough to deserve attention.

Despite the characteristic thrust behaviour of the fault, there is no reason to assume that it is strictly dip-slip. A strike-slip component of motion may exist. To introduce a lateral component of relative displacement, one must adopt a convention about its sign, and hence about the angle α. We count the angle α in the clockwise sense from the right side of the fault, as seen from any of the blocks (Fig. 6). This angle α is 57° at sub-site A and 120° at sub-site B. We define a left-lateral displacement positive, a right-lateral one negative. Along the strike of a rectilinear feature, the apparent shortening, S, is thus given by the sum of two terms. The first term is the same as in Eq. (1), and reflects the influence of the fault-perpendicular component of horizontal displacement. Shortening being counted positive, this term is positive. The second term depends on the amount of fault-parallel horizontal displacement, L. It may be positive or negative. One thus obtains:

$$S = T\sin\alpha - L\cos\alpha \quad (2)$$

For an angle α smaller than 90°, the shortening of the rectilinear feature is smaller than that expected for a dip-slip fault if the displacement has a left-lateral component ($L > 0$; compare Fig. 6a and b). It is larger if the displacement has a right-lateral component ($L < 0$; compare Fig. 6a and c). Because Eq. (2) contains two unknowns, T and L, one cannot determine the fault displacement by measuring the shortening along a single rectilinear feature. If two non-parallel rectilinear features are offset by the fault, both the unknowns T and L can be determined. With indexes A for sub-site A and B for sub-site B, one writes:

$$S_A = T\sin\alpha_A - L\cos\alpha_A \text{ and } S_B = T\sin\alpha_B - L\cos\alpha_B \quad (3)$$

This system of two equations allows determination of T and L as follows:

$$T = (S_A\cos\alpha_B - S_B\cos\alpha_A)/\sin(\alpha_A - \alpha_B) \quad (4)$$

$$L = (S_A\sin\alpha_B - S_B\sin\alpha_A)/\sin(\alpha_A - \alpha_B) \quad (5)$$

With the values already mentioned for S (1.92 ± 0.14 and 2.53 ± 0.18 m) and α (57 and 120°), at sub-sites A and B, respectively, one obtains 2.62 ± 0.19 m for the transverse component of horizontal fault displacement, T, and 0.52 ± 0.30 m for the strike-slip component, L. The latter value is positive, indicating a left-lateral sense (Table 1).

The vertical offset, V, is 2.65 ± 0.20 m on average. Knowing the three components of fault slip, other values can be calculated by using the Pythagorean theorem in two and three dimensions. The total slip is 3.77 ± 0.32 m. Because the lateral offset is minor, the dip-slip component is almost the same (3.73 ± 0.28 m). The comparison between the left-lateral and dip-slip components of fault displacement yields a pitch of 82 ± 5° to the SE for the slip on a N141°E striking fault surface. The slope of the near-surface fault is obtained as the ratio between the vertical and transverse horizontal components of relative displacement. It corresponds to a dip angle of 45 ± 4°, an acceptable value for a reverse fault coming to the surface. Based on the ratio between the lateral and transverse components of the horizontal relative displacement, the slip azimuth makes an angle of 79 ± 7° anticlockwise with the N141°E average fault strike. This indicates a N62°E (±7°) trend of the slip vector (footwall relative to hanging wall). The horizontal shortening in this direction is 2.67 ± 0.25 m.

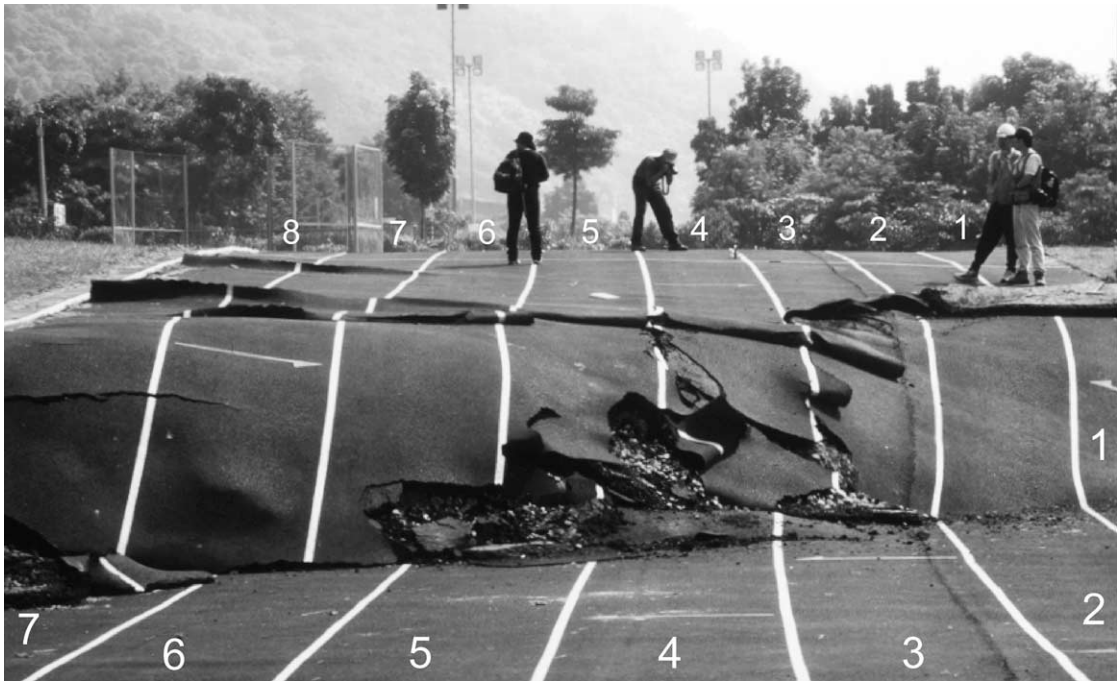

Fig. 7. Photograph of fault scarp of the September 21st earthquake, 1999, at sub-site B. Location in Fig. 4. View towards E, from footwall towards hanging wall. Stadium tracks numbered 1–8. Note the apparent right-lateral displacement of painted lines separating tracks, despite a left-lateral slip component (compare with map of sub-site B in Fig 4c; also see Fig. 9c). Same situation as in Fig. 6c, except for benchmark trend (E–W) and fault strike (NW–SE).

4. Determination of fault slip based on three-component displacement (sub-site B)

The above determination is underlain by the assumption that the fault slip is the same at sub-sites A and B. As a consequence, this determination may be affected by a possible variation in the orientation of fault slip between the two sub-sites. Because the stadium tracks were rectilinear at sub-site B (Figs. 3a and 4), not only could we measure their shortening, S, but also their displacement, D, in the direction perpendicular to track strike (the difference, 5°, with the profile strike can be neglected). For a dip-slip fault (Fig. 6a), D would be given by:

$$D = T\cos\alpha \tag{6}$$

With the same conventions as before concerning α and L, one also determines this offset if the fault is not dip-slip. D is given by the sum of two terms: the value of Eq. (6), obtained for a dip-slip fault, and the component of L in the direction perpendicular to the rectilinear feature:

$$D = T\cos\alpha + L\sin\alpha \tag{7}$$

For an angle α smaller than 90°, the apparent offset, D, of the rectilinear feature in the direction perpendicular to its strike is larger than that expected for a dip-slip fault if the slip has a left-lateral component ($L > 0$; compare Fig. 6a and b). It is smaller for a right-lateral component ($L < 0$; compare Fig. 6a and c). If both S and D can be measured, combining Eqs. (2) and (7) allows determination of the two unknowns, T and L, in a single sub-site:

$$L = D\sin\alpha - S\cos\alpha \tag{8}$$

$$T = S\sin\alpha + D\cos\alpha \tag{9}$$

At sub-site B, the shortening S in the N81°E direction has already been determined (2.53 ± 0.18 m). The value of D was measured for nine N86°E track-bounding lines (Fig. 7), giving an average displacement of 0.83 ± 0.10 m in the right-lateral sense (and hence a negative D). One thus obtains, with the value of 120° for α, 0.55 ± 0.18 m for L (positive, indicating a left-lateral component of slip) and 2.61 ± 0.21 m for T. These results resemble those obtained in the previous sub-section (Table 1). Remember that these values were determined through consideration of a single parameter at two sub-sites in the first case, and of two parameters in a single sub-site in the second case.

The geometry of the earthquake fault surface slip at sub-site B can be completely determined. The vertical offset, V, is 2.87 ± 0.22 m. With the values of T and L given above, one obtains a total slip of 3.92 ± 0.33 m and a dip-slip component of 3.88 ± 0.20 m. The pitch on the N141°E striking fault surface is 82 ± 3°, and the dip angle of the fault is 48 ± 4°. One also determines an angle of 78 ± 5° anticlockwise between the slip azimuth and the N141°E fault strike. This indicates a N63°E (±5°) trend of the slip vector, with a horizontal shortening of 2.67 ± 0.24 m in this direction.

Note, incidentally, that at the sub-site B the apparent offset of the painted lines of the stadium tracks is right-lateral

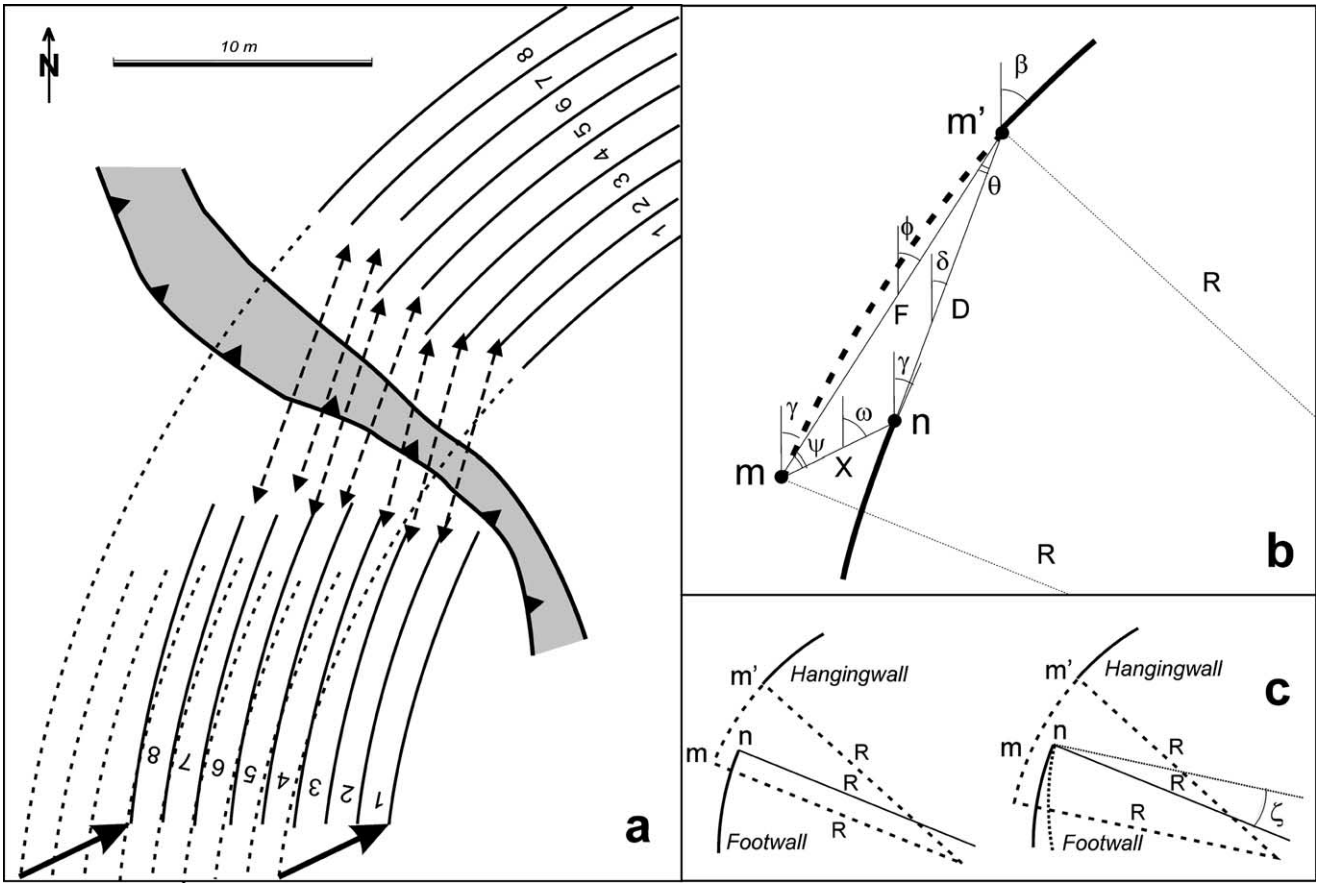

Fig. 8. Determination of the horizontal fault displacement of the September 21st earthquake, 1999, at sub-site A. Calculation based on the comparison between painted lines of elliptical stadium tracks in footwall and hanging wall. Location in Fig. 4. Observed and calculated values in Table 2 and text. (a) Map of sub-site A. Fault zone in grey; measured segments as dashed lines with arrowheads (not to scale). Horizontal component of displacement vector as solid arrows. (b) Geometrical analysis (explanation and symbols in text). Painted line as thick black line. (a) Change in geometrical scheme for additional rotation by an angle ζ. In hanging wall, reconstructed portion of ellipse and radii as dashed lines. In footwall, observed portion of ellipse and radius as solid lines, back-rotated portion of ellipse and radius as dotted lines.

(Fig. 7), whereas the actual strike-slip component of fault displacement is left-lateral. This geometrical configuration provides a good example of elementary pitfall for students in structural geology.

5. Use of elliptical benchmarks to determine fault displacement (sub-site A)

We also entirely constrained the fault slip geometry at sub-site A (Fig. 3a), where the rupture trace crosses the western ellipse of the stadium (Fig. 4). Taking advantage of the elliptical pattern of stadium tracks, it is possible to determine the relative displacement of the two blocks, although the geometrical restoration is more complicated than before. By determining the shape and the position of an elliptical painted line on both sides of the fault zone, one reconstructs the shift between the two portions of the broken half-ellipse (Fig. 8a).

For each painted line, we chose two points, n (footwall) and m′ (hanging wall), near the tips of the intact painted lines on both sides of the deformed zone (Fig. 8b). We measured the length, D', and the azimuth, δ, of the segment m′–n. The corresponding horizontal distance, D, was derived from D' by considering the vertical offset (2.43 m) between the two blocks. Prior to the earthquake, the two points belonged to the same painted line but were separated by an unknown distance along this ellipse. The azimuths of the line at these two points, γ at n and β at m′, were measured (Fig. 8b). It was necessary to determine the local radius, R, of each elliptical track at sub-site A. Because the deformed zone is narrow, we considered the circle that tangents and best fits the ellipse in A, rather than the ellipse itself. The radius of the circle was measured through comparisons with the equivalent undamaged portions of the stadium (Fig. 4a and b). The data collection was independently done for seven painted lines separating the eight stadium tracks. For each of these broken lines, the measured parameters are listed in Table 2. The internal structure of the deformation zone was ignored in this approach.

The steps of the geometrical analysis are shown in Fig. 8b. To reconstruct the original arc of painted line in the

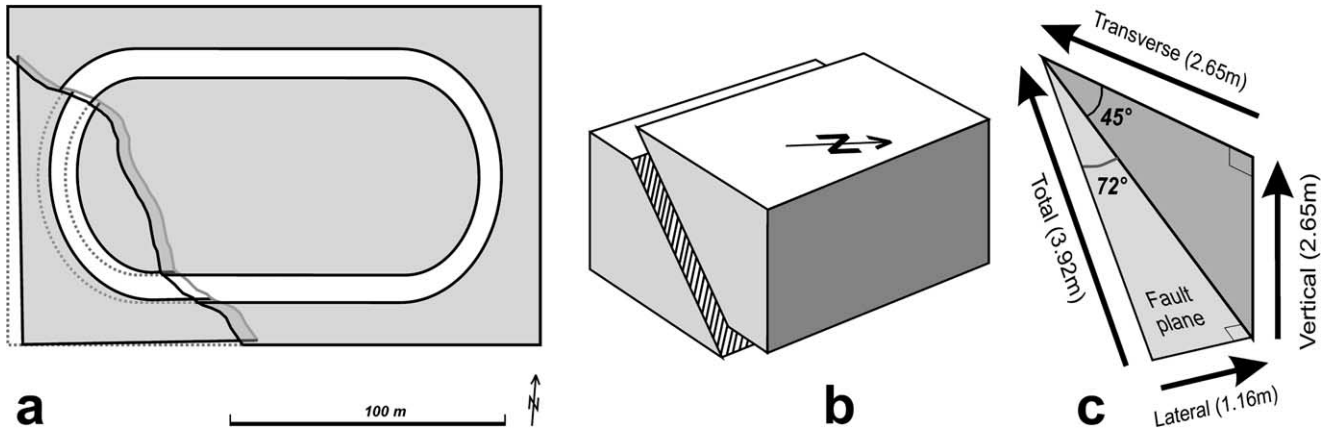

Fig. 9. General results of the determination of fault displacement of the September 21st, 1999, earthquake in the Kuangfu stadium. (a) Map of the hanging wall and footwall blocks. Grassy areas in grey, stadium tracks left white. Initial position of footwall relative to hanging wall indicated by dotted lines. Note the 1° anticlockwise rotation (footwall relative to hanging wall). (b) Block showing the reverse motion with minor left-lateral component of the fault. (c) Main components of the relative fault displacement, with dip angle and pitch of slip vector indicated for a N141°E fault strike. Averaged values (details in Table 1).

hanging wall, one finds the position of a virtual point, m, that corresponds to the point m′ observed in the footwall. Assuming that at the scale of the stadium the fault displacement is a rigid translation, two unknowns describe the horizontal component of relative displacement: the amount, X, and the azimuth, ω (footwall relative to hanging wall). The difference between the azimuths β and γ directly gives the angle of the corresponding sector of circle, prior to the earthquake. We thus calculate the chord length, F, for the original arc of radius R that connected the observed and reconstructed points of the hanging wall (m′ and m, respectively, in Fig. 8b):

$$F = 2R\sin([\beta - \gamma]/2) \tag{10}$$

The azimuth, ϑ, of this segment m–m′ is given by:

$$\varphi = (\beta + \gamma)/2 \tag{11}$$

As a result, the angle, θ, between the segments that connected the two points of the arc prior to the earthquake (the calculated segment m–m′, characterised by F and ϑ) and after the earthquake (the observed segment n–m′, known from D and δ) is given by:

$$\theta = \varphi - \delta \tag{12}$$

Both the lengths and the trends of homologous pre- and post-earthquake segments, m–m′ and n–m′, respectively, are thus known. The third side of the mm′n triangle, m–n, connects the observed point of the footwall and the homologous calculated point of the hanging wall. It thus represents the horizontal component of the relative displacement vector. The extended Pythagorean theorem gives the length, X, of this displacement vector:

$$X^2 = D^2 + F^2 - 2DF\cos\theta \tag{13}$$

The angle, ψ, between the chord and this third side of the triangle is given by:

$$X\sin\psi = D\sin\theta \tag{14}$$

The azimuth, ω, of this third side is:

$$\omega = \varphi + \psi \tag{15}$$

The numerical application allowed us to determine seven vectors (Table 2), giving an average displacement and standard deviation of 3.36 ± 0.71 m in the direction N83°E ± 15° (footwall relative to hanging wall). Although the amount of horizontal relative displacement is about 25% larger, and despite the 23° difference between the slip trends resulting in a larger strike-slip component, the values obtained in this third determination remain generally compatible with the previous ones considering the uncertainties (Table 1).

We considered the possibility of horizontal block rotation by an angle ζ (Fig. 8c). The simplest way to introduce such a rotation consists of modifying the value of γ. One thus performs a back-rotation (by an angle $-\zeta$) of the footwall relative to the hanging wall, before undertaking the geometrical determination process presented before. Minor corrections were added to consider the rotation between two rigid blocks rather than independent identical rotations for all painted lines. In the field, the observation of the broken western half-ellipse of the stadium suggested that during the earthquake the hanging wall had locally undergone a clockwise rotation of about one degree, relative to the footwall. With this value, the modified calculation yielded an average displacement of 3.09 ± 0.60 m in the direction N92°E ± 15° (footwall relative to hanging wall). This result is compatible with the previous one (compare A_1 and A_2 in Table 1). This minor rotation is incorporated in the reconstruction of Fig. 9a.

Thus, the geometry of the earthquake fault slip could be completely reconstructed at the single sub-site A. We adopt the values obtained for X (3.36 ± 0.71 m) and ω

(N83°E ± 15°) under the assumption of simple rigid translation. With the N141°E average fault strike, one obtains 2.85 ± 1.04 m for the transverse component of horizontal fault displacement, *T*, and 1.78 ± 1.10 m for the strike-slip component, *L*. Taking the vertical offset, *V*, into account (2.43 ± 0.18 m), the fault dip is 40 ± 13°, the dip-slip component is 3.75 ± 0.90 m and the pitch of the slip vector is 65 ± 19° to the SE. This fault geometry does not markedly differ from the previously reconstructed ones, although the more oblique orientation of slip implies a larger left-lateral component of slip (Table 1).

6. Discussion and conclusions

The results presented above deserve examination in several respects. (1) To evaluate the confidence that can be given to local determinations of co-seismic displacement, is it possible to determine the origin of the discrepancies? Do errors result from structural differences between sub-sites, or from differences in methods? (2) Is it possible to combine and synthetise the results at the scale of the Kuangfu school site, in terms of translation and rotation of the two fault blocks during the Chichi earthquake? (3) Is the flexure that developed on the hanging wall side during co-seismic faulting related to a variation of fault dip with depth? (4) Considering the response of the surface scarp zone to faulting, are sophisticated geometrical analyses indispensable, or would simpler models provide equivalent results? (5) Do the determinations of the co-seismic fault displacement at Kuangfu reflect the far-field information on the displacement pattern of the Chichi earthquake? (6) Does partitioning occur across the Chelungpu fault zone? (7) Is it possible to draw regional inferences from this site, or should it be regarded atypical? (8) How is the apparent dip angle of surface faults related to that of the underlying thrust?

The present paper is mainly devoted to methodological concerns about determination of co-seismic fault slip in the field. For this reason, emphasis is put on aspects (1–5) and (7 and 8), whereas the partitioning phenomenon (6) is discussed elsewhere (Angelier et al., 2002).

6.1. Significance of minor discrepancies

Two full determinations of the fault relative displacement have been independently carried out in the Kuangfu stadium (lines B and A_1–A_2 in Table 1). The determination at sub-site B (Section 4 and Fig. 3b) was based on consideration of the along-strike and across-strike components of displacement (Fig. 6), using Eqs. (8) and (9). It indicates a horizontal displacement of 2.67 m in the N63°E direction (footwall relative to hanging wall). For the determination at sub-site A (Section 5 and Fig. 3a), we matched elliptical benchmarks in the stable domains on both sides of the fault (Fig. 8), using Eqs. (10)–(15). The calculated displacement was 3.36 m in the direction N83°E (without rotation), or 3.09 m in the direction N92°E (with a 1° rotation). Taking uncertainties into account, these local results are compatible in the first approximation.

The fault relative displacement was also determined through a comparison between the two sub-sites involving consideration of a single parameter, the shortening of a rectilinear benchmark (Section 3). This result and that obtained at sub-site B were almost identical (lines A–B and B in Table 1). This similarity suggests, but does not demonstrate, that the fault behaviour is the same in both places. Because the two determinations share one datum, the amount of E–W shortening in B, they cannot be regarded fully independent.

The procedure adopted at sub-site A (Fig. 8) yielded the horizontal component of the displacement vector without any reference to the fault orientation (Table 1, lines A_1 and A_2). The direction and amount of horizontal displacement, ω and *X*, were directly determined and allowed subsequent calculation of the transverse and lateral horizontal components of slip, *T* and *L*. In contrast, in the other two determinations (Table 1, lines A–B and B), the displacement components *T* and *L* were calculated first and the horizontal component of slip was derived later. Not only are these two procedures independent in terms of the sub-sites where they were applied, but also they markedly differ in their geometrical principle.

In terms of fault slip geometry, differences between the two sub-sites may exist but remain minor, and are unlikely to account for the differences in the results of Table 1. This conclusion is supported by simple observations. For instance, from A to B, the vertical and horizontal relative displacements vary in opposite senses (Table 1). Also, the minor rotation suspected (1° clockwise, hanging wall relative to footwall) would imply a larger horizontal displacement in sub-site B as compared with A, which is not the case (Table 1). This rotation principally results from a local behaviour of the hanging wall (and partly of the surface layer). In the first approximation the same fault deformation affected the two sub-sites.

The main difference in the results lies between A–B and B on one side, and A_1 and A_2 on the other side (Table 1). In the first case, the fault slip geometry was determined mainly based on observations inside the fault zone (Fig. 6). This first determination mode may be affected by errors in deformation estimates. In the second case, the fault slip geometry was obtained by matching some geometrical patterns of the stable blocks outside the fault zone (Fig. 8). This second determination mode is subject to larger uncertainties, but has no dependence on the internal structure of the fault zone. One concludes that the second-order discrepancy between these determinations results is mainly a consequence of the difference in the geometrical approaches adopted in A and B.

6.2. Homogeneity of results

From this comparison between the results obtained in

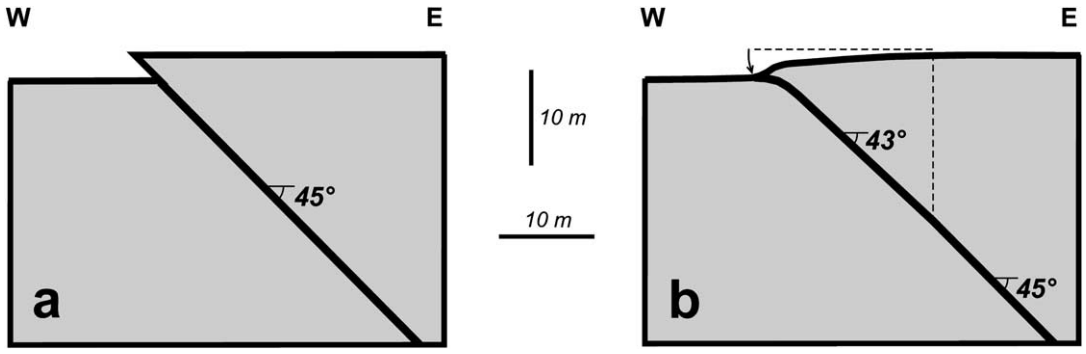

Fig. 10. Deformation of the hanging wall of the September 21st, 1999, earthquake fault in the Kuangfu stadium. Schematic cross-sections perpendicular to fault strike. (a) Reconstructed cross-section without hanging wall deformation. (b) Actual cross-section showing flexing of the edge of the upper block over a width of 10–20 m and a height of about 1 m. Compare with topographic profiles of Fig. 5, taking into account their 57–60° obliquity to fault strike.

Sections 3–5 a question arose: might the shortening at sub-site B be underestimated? One may formulate the hypothesis of unnoticed compressive deformation, continuous in type, in the deformed synthetic surface layer of the stadium tracks. Such an undetectable deformation would have led us to underestimate the fault displacement in B. This is an important issue, because the presence of undetected deformation would affect estimates of co-seismic displacement at many localities along the Chelungpu Fault, resulting in systematic underestimation.

Note that by definition the analysis carried out in sub-site A cannot be affected by such a bias, because it relies on benchmarks away from the scarp and thus does not depend on the deformation pattern inside the rupture zone (Section 5). For this reason, we re-calculated the shortening along the profiles at sub-site A, with the results listed in Table 1 (line A_1). Along the N18°E direction of the profiles, Eq. (2) predicts a shortening, S, of 1.42 ± 1.47 m, less than the shortening of 1.92 ± 0.14 m measured along the profiles. Considering the uncertainties, the values fall in the same range. The same calculation was done for the average direction of the stadium tracks at sub-site A, N31°E. It gave 2.02 ± 1.37 m for S and 2.68 ± 1.40 m for D, based on Eqs. (2) and (7), respectively. Not only is the shortening, S, compatible with the measured values, but also the calculated left-lateral offset of the tracks, D, is compatible with that estimated in the field at sub-site A. This observed offset, 3.1 ± 0.6 m, is by 16% larger than the calculated one, which falls within the range of uncertainties.

Two conclusions are drawn from these comparisons. First, our determination of fault displacement at sub-site A (Section 5) is confirmed by an independent offset estimation as mentioned above. Second, because the predicted profile-parallel shortening generally fits the observed one (and in detail is even smaller), there is no reason to suppose that unnoticed compression has affected our measurements of the profile-parallel shortening. In light of this conclusion, more confidence can be given to other determinations of the earthquake fault slip.

At sub-site B, it appears that with the same fault dip angle as in A, the shortening would be larger than that actually measured. Keeping the same ratio between the transverse and vertical offsets would imply in B a fault perpendicular shortening of about 3.4 m, 30% more than that of Table 1. A slightly underestimated shortening in B would thus well account for the discrepancy between the determinations of the horizontal component of fault slip (about 2.7 m in B and 3.2 m in A; see Table 1). In contrast with sub-site A, no independent observation confirmed our determination at sub-site B. On the other hand, in A, the accuracy was less. The discrepancy is in any case acceptable within the range of uncertainties.

The above discussion has implications for the rotation of about 1° already mentioned. Such a clockwise rotation (hanging wall relative to footwall) requires a larger horizontal displacement in sub-site B, as compared with A. The distance between the two sites is about 70 m. The vertical offset is approximately 18% larger in B than in A. Assuming identical fault dip, the transverse shortening would be larger by the same proportion. The pole of a rigid rotation between the two blocks would thus be located at a distance of about 450 m NNW of sub-site A. The fault scarp height effectively diminishes inside the ruined school (Fig. 2), NW of sub-site A. Although no accurate measurement of fault displacement could be made in this area, this variation is qualitatively consistent with the proposed rotation (Fig. 9a). The only evidence that contradicts this interpretation is the relatively small amount of shortening observed along the N86°E stadium tracks at sub-site B.

However, the local variations in fault geometry are certainly more complex than those involved by a rigid rotation. We observed minor rupture traces of the same earthquake north of the stadium, indicating that the co-seismic deformation was larger, and more complicated, than that revealed by the stadium fault. We come back later to this aspect, based on consideration of the geodetic results available in the surrounding area.

All the variations discussed above are second-order ones. In the first approximation (Fig. 9), the determinations presented in this paper concur to demonstrate that in the

Kuangfu stadium the N141°E trending fault is a left-lateral reverse fault that dips 45°NE. The pitch of the slip vector is 72°SE and the average vertical offset is 2.65 m. Based on these values, the horizontal components of relative displacement average 2.65 m (*T*, transverse) and 1.16 m (*L*, lateral), giving a total displacement of 3.92 m. The average horizontal component of the slip vector is 2.89 m in the N75°E direction (footwall relative to hanging wall).

6.3. Flexuring in hanging wall edge zone

In cross-section (Fig. 10), the deformation on the hanging wall side of the fault is intriguing. Because all our calculations were based on consideration of the total vertical and horizontal components of displacement, they revealed the fault behaviour at the scale of a few hundred metres, indicating a dip angle of about 45° (Fig. 10a).

However, the topographic profiles revealed significant footwall-verging flexing in the hanging wall block, within distances of 10–20 m from the base of the scarp (Fig. 5). The tilt angle is almost 3°, resulting in a vertical offset of about 0.5–1 m. Considering the subsurface in the 0–100 m range, the scale of this study, the hanging wall deformation indicates that below a depth of 10–20 m the fault is about 2° steeper than above (Fig. 10b). The dip angle of 45° thus describes the configuration at depths larger than 10–20 m, whereas at shallower depths the fault probably dips 43° or less. Furthermore, these dip angles are certainly not maintained in the first metres below the surface, where a shallower fault dip is expected (Fig. 10b). This upward-convex shape of the fault fulfils a simple geometrical requirement considering the deformation of the edge of the hanging wall in the smoothed scarp zone (Figs. 3 and 5).

Considering larger depths, these dip angles are certainly not valid in the upper crust. The earthquake source study showed the main shock as a thrust faulting along a plane dipping 25°E down to at least 15 km depth (Kao and Chen, 2000). At intermediate depths of 1–7 km, the structural reconstruction of balanced cross-sections within the sedimentary pile suggested important changes in fault dip, with a generally upward-concave shape as Fig. 1d shows. In detail, the fault shape may be affected by the presence of inherited normal faults, undergoing reactivation during the collision-related compression (Mouthereau et al., 2001a,b).

All these determinations at different depths indicate that the Chelungpu fault cannot be regarded as a planar fault and that variations of at least 20° affect its dip angle. Larger variations even exist, according to field analyses indicating dip angles steeper than 50° (Lin et al., 2001). On the other hand, a dip angle of 30° is documented at a place where the fault is a typical N–S-trending west-verging thrust (Angelier et al., 2002). At several places along the 80-km-long N–S portion of the fault trace, we observed local evidences for steeply dipping faults. Some of these faults trend N–S, parallel to the regional thrust, and show nearly dip-slip displacement, indicating that they accommodate vertical motion near the thrust. Other steep faults trend oblique to the regional thrust, and show nearly strike-slip displacement, related to a variety of phenomena (conjugate strike-slip faults, transfer faults, hanging wall partitioning).

At Kuangfu, the uppermost 10–20 m being left apart, our determination of fault dip in the range 40–45° is probably valid in the uppermost 100 m. At larger depths, the fault progressively flattens, with dips decreasing to 20–30° towards the focal area, and farther east probably merges into a flat detachment beneath the Central Range (Fig. 1d).

6.4. Limitations of simple models

An aspect that was noticed but not quantitatively taken into account in the previous sections is the particular behaviour of the synthetic surface layer employed to build the stadium tracks. Although its mechanical response to faulting generally resembles that of an asphalted surface, the lower adherence and higher internal cohesion of the artificial layer used in the stadium resulted in systematic décollement in the fault zone and geometrically consistent folding with relatively little rupturing and tearing (Fig. 3). Tight geometrical constraints, which were not used above, result from this specific behaviour.

Although the fault scarp is generally sinuous, it shows nearly identical strikes, N128°E on average, in both sub-sites (Fig. 4). This strike differs from the N141°E average strike of the fault in the stadium area. Assuming that the geometrical integrity of the folded surface cover has been preserved, one may imagine a N38°E trend of the co-seismic relative displacement, perpendicular to N128°E fold axes. This is not acceptable, because the surface cover has undergone substantial tearing although its continuity was generally maintained (Fig. 3). Tight metric folds developed, with axes nearly perpendicular to tear faults. They can be observed in the footwall (Fig. 3a) as well as the scarp and hanging wall (Fig. 3b). Because they trend oblique to the scarp and are more or less en-échelon, these structures accommodate the left-lateral component of deformation. As a consequence, a simple model of fault-parallel folding would be incorrect and fail to account for the actual co-seismic deformation. In other words, the co-seismic relative displacement in the surface layer involved not only scarp-perpendicular shortening but also left-lateral shear absorbed by tear faults and tight folds.

At sub-site B, the height of the scarp is 2.87 m and its average dip angle is about 38°. This represents a shortening of 1 m in the direction N38°E, perpendicular to scarp strike. The tear fractures and the tight folds are roughly parallel and perpendicular, respectively, to the stadium tracks (Fig. 3b). They indicate a shortening of about 1.8 m in the N86°E direction. By adding the two vectors, one obtains a total horizontal displacement of 2.6 m in the N69°E direction. This is almost the same vector as that determined at sub-site B (2.7 m in the N63°E direction). Similar conclusions can be drawn at

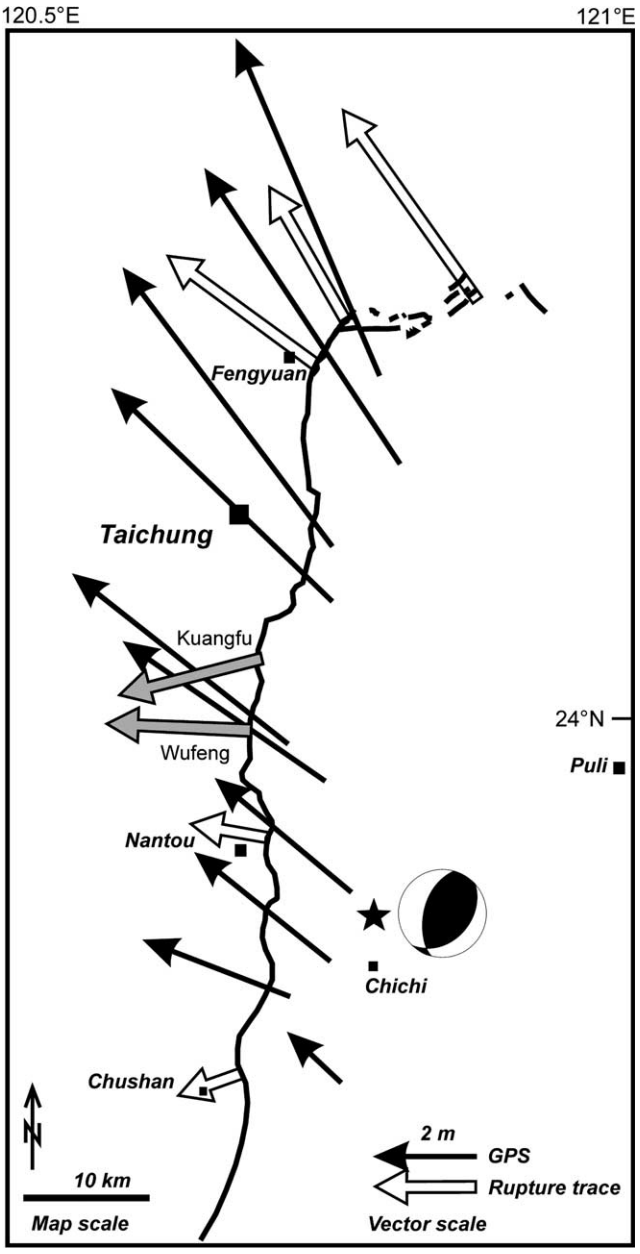

Fig. 11. Distribution of displacement along the Chelungpu Fault during the September 21st, 1999, earthquake (simplified). Fault trace as black line, epicentre of Chichi earthquake as star (with mainshock focal mechanism as beachball stereoplot). GPS data from Central Geological Survey (1999b) and Yu et al. (2001), indicating displacement of hanging wall stations at distances less than 7 km from the rupture trace, with respect to the stable foreland (solid arrows). Data along the fault trace from Lee et al. (2001) for white open arrows, Angelier et al. (2002) and this paper for grey open arrows.

sub-site A, although the deformation in the synthetic surface layer is complex (Fig. 3a). This consistency shows that a model based on consideration of the geometrical integrity of the surface layer is correct provided that the horizontal simple shear is not ignored. It brings indirect confirmation that the determinations of co-seismic slip vectors presented in this paper are valid.

6.5. Comparison with far-field information

The significance of the result obtained at Kuangfu also deserves examination with respect to the kinematics of the Chichi earthquake. Geodetic (GPS) studies resulted in an excellent knowledge of the deformation pattern for this major earthquake, and the results fit very well with a relatively simple model of co-seismic deformation (Hou et al., 2000; Johnson et al., 2001; Yu et al., 2001). A selection of horizontal displacement vectors close to and along the front of the Chelungpu thrust unit (Fig. 1) is shown in Fig. 11. Some vectors are issued from GPS studies, for stations located in the hanging wall, at distances less than about 7 km from the rupture trace. These vectors are NW-directed on average, but display a fan-shaped pattern, with NNW trends in the northern region, near Fengyuan, and WNW ones to the south, near Nantou. Other vectors refer to the relative displacement determined in the field along the rupture trace of the Chichi earthquake, including the two vectors obtained in the Kuangfu stadium (this paper) and the Wufeng car park (Angelier et al., 2002). The vectors, which are NW-directed near Fengyuan and W-directed near Nantou, also show a fan-shaped pattern. Moreover, the two sets of vectors show a similar along-trace variation in relative displacement amplitude. Based on GPS studies, the hanging wall displacement is 6–7 m near Fengyuan and 3–4 m near Nantou. Along-trace analyses indicate relative displacements of about 4 and 2 m in the same regions (respectively). The decrease rate, from north to south, is the same for the two sets of vectors, that is, about 50% for a N–S distance of 40 km. To these respects, all these displacement data reveal high levels of consistency, which suggests that they fairly well represent the general motion of the Chelungpu thrust during the Chichi earthquake.

On the other hand, comparing the absolute values, a striking contrast occurs between the displacement data issued from the GPS surveys and those obtained along the rupture trace, in terms of both the trends and the amplitudes. The horizontal slip component measured along the rupture trace shows systematic anticlockwise deviation and smaller amplitude with respect to the GPS-based vectors obtained at larger distances from the rupture trace (Fig. 11). In terms of angular deviation, the difference averages 20° near Fengyuan and 30–40° near Nantou. In terms of amplitudes, the along-trace displacement roughly represents one half of the far-field displacement in both regions. In the horizontal displacement pattern of Fig. 11, the GPS data refer to displacements in the upthrust unit with respect to the stable foreland, whereas the rupture trace data refer to the displacement of hanging wall relative to footwall across the surface rupture (that is, the fault slip). A full comparison requires additional consideration of the GPS-based displacement data in the footwall, to obtain the far-field relative displacement vectors across the entire belt front zone (Fig. 1). This correction does

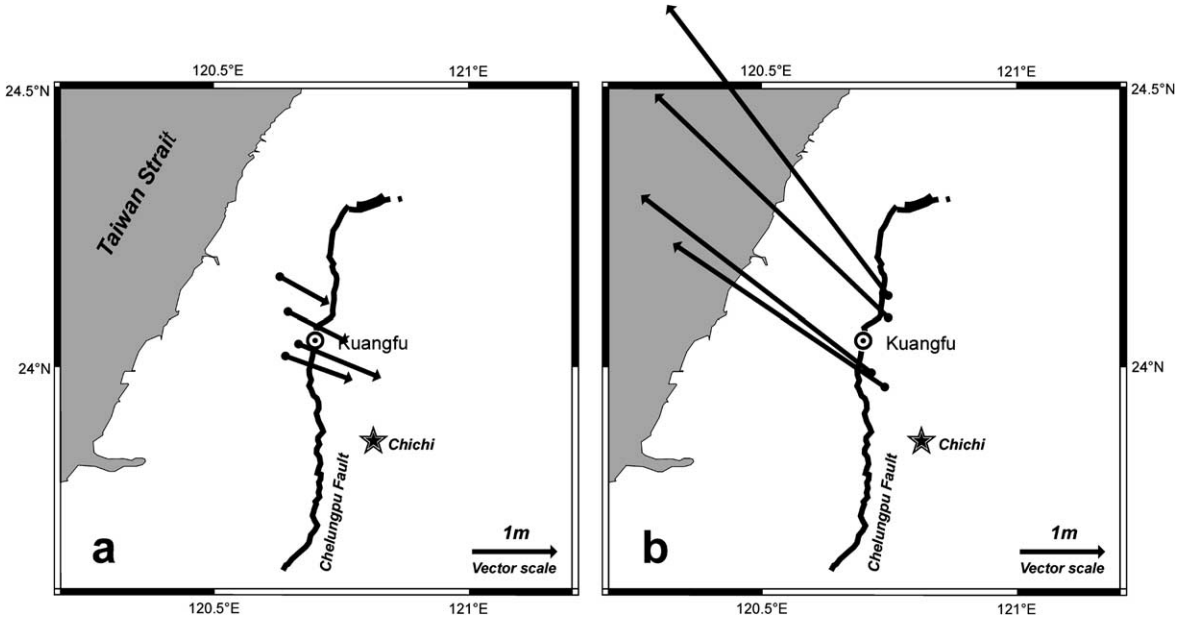

Fig. 12. Horizontal relative motion of the September 21st, 1999, earthquake near Kuangfu. Data extracted from GPS geodetic surveys before and after the earthquake (Hou et al., 2000; Yu et al., 2001). Selection of eight stations on footwall (a) and hanging wall (b) of the Chelungpu Fault. Epicenter as framed star, rupture trace as thick line, Kuangfu school as circle with dot.

not markedly affect the trend distribution, and results in a slightly larger contrast in terms of amplitudes.

To evaluate in more detail the distribution of the deformation related to the Chichi earthquake in the Kuangfu region, we have selected the results from eight geodetic (GPS) stations operated by the Central Geological Survey and the Academia Sinica of Taiwan. The geodetic networks were surveyed before and after the Chichi earthquake (e.g. Yu et al., 1997, 2001; Hou et al., 2000). Four stations are located on the footwall block, at distances of 2–15 km from the Kuangfu school (Fig. 12a). Their co-seismic displacements are in the range 0.72–1.10 m, in the directions N114–122°E. The other four stations are located on the hanging wall block, at distances of 7–11 km from the Kuangfu school (Fig. 12b). Their co-seismic displacements are in the range 3.1–4.4 m, in the directions N38–55°W. All

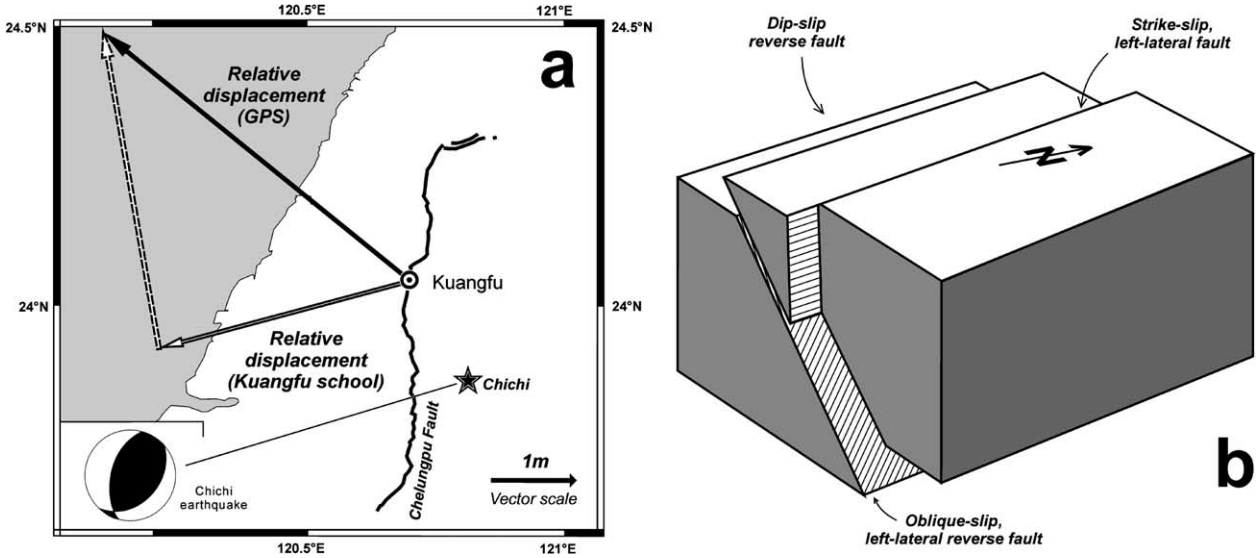

Fig. 13. Fault slip and far-field deformation of the September 21st, 1999, earthquake in Kuangfu. Comparison between determinations of relative displacement on fault trace (this paper) and in surrounding geodetic stations (see Fig. 12). (a) Horizontal components of relative displacement vectors, hanging wall relative to footwall. Average vector from GPS analyses as solid black arrow, average fault slip vector in the Kuangfu stadium as open arrow, remaining vector as dashed arrow. Values in text. Epicentre of earthquake as star, rupture trace as thick line, Kuangfu school as circle with dot. Focal mechanism of earthquake as in Fig. 1. (b) Block diagram illustrating the inferred slip partitioning.

Table 2
Numerical application of the method using elliptical benchmarks to determine the horizontal component of fault displacement (Fig. 8a). All symbols described in text and Fig. 8b. No rotation. Lengths (uppercase letters) in metres. Angles (Greek lowercase letters) in degrees. Measured values: R, D' (and hence D), β, γ and δ. Calculated values: F, ϑ, θ, ψ, X and ω, given by Eqs. (10)–(15)

R	D'	D	β	γ	δ	F	ϑ	θ	ψ	X	ω
30.26	8.60	8.25	41	25	14	8.42	33	19	77	2.76	110
31.51	8.72	8.37	40	23	13	9.31	32	19	63	2.99	94
32.75	7.90	7.52	39	23	12	9.12	31	19	51	3.17	82
34.00	9.05	8.72	41	23	18	10.64	32	14	44	3.03	76
35.25	9.28	8.96	39	22	16	10.42	31	15	52	2.84	83
36.50	10.39	10.10	43	21	17	13.93	32	15	32	4.92	64
37.75	11.37	11.11	41	20	18	13.76	31	13	40	3.78	70

these values indicate high consistency of the results, with average displacements of 0.9 m in the N118°E direction for the footwall side and 3.7 m in the N48°W for the hanging wall side.

Building the velocity triangle, one infers that the relative displacement between the two blocks near Kuangfu is 4.6 m in the direction N51°W (hanging wall relative to footwall). The same calculation applied to the two stations closest to Kuangfu (2.8 km to the W and 7 km to the SSE) yields a similar result, 4.6 m in the direction N49°W. This relative displacement vector is shown as a solid arrow in Fig. 13a. There is a striking contrast between this determination and the relative displacement determined across the Kuangfu stadium fault, 2.9 m in the S75°W direction on average (open arrow in Fig. 13a). Not only does the horizontal shortening in the stadium scarcely represent two thirds of the total relative motion across the Chelungpu fault zone at this latitude, but also its direction shows an anticlockwise deviation as large as 56° with respect to the horizontal component of displacement in this region. Building again a finite velocity triangle, it is easy to determine the additional displacement vector required to fit the GPS-based shortening. This vector is 3.8 m long in the direction N10°W (hanging wall relative to footwall). It is shown as a dashed arrow in Fig. 13a.

Two conclusions emerge from these comparisons. First, a very significant proportion of the total displacement is accommodated outside the rupture trace observed in the stadium. We observed several secondary fractures of the Chichi earthquake near the Kuangfu school, especially north of the stadium area. These fractures indicate that significant co-seismic deformation has affected the upthrust unit within distances of a few hundred metres from the main rupture trace, as was noted at many other places along the Chelungpu Fault. Despite the lack of accurate measurements, this deformation certainly accounts for a substantial amount of additional displacement. The proportion absorbed at larger distances of the fault is not documented by field studies in this area. The second conclusion deals with the almost N-orientation of the inferred component of displacement (Fig. 13a). Its trend, N10°W, is nearly perpendicular to the trend of the Kuangfu school displacement vector, S75°W. It is also approximately parallel to the regional trend of the Chelungpu Fault, indicating a left-lateral sense. These angular relationships argue in favour of slip partitioning (Fig. 13b).

6.6. Fault partitioning

At shallow depths, two types of shear accommodated the oblique slip of the fault: nearly dip-slip thrusting across the rupture trace, as observed in the Kuangfu stadium, and left-lateral strike-slip in the hanging wall block, probably distributed along multiple fracture zones. At larger depths, the shear zones merge into a single, oblique-slip fault (Fig. 13b). The most spectacular surface expression of the earthquake rupturing process was a west-verging thrust with a minor strike-slip component as observed in Kuangfu (Fig. 9c). Most of the left-lateral shear required by the deep oblique thrusting was distributed east of the fault, within a distance smaller than 5 km. For this reason, the displacement vectors in the neighbouring geodetic stations (Fig. 12b) show no significant anticlockwise deviation relative to the displacement field farther east. The thrust fault and the left-lateral shear zone probably delineate a deformed, horizontally elongated prism with a triangular section (Fig. 13b). High co-seismic deformation took place in this hanging wall edge zone where widespread fissuring and damage occurred, in contrast with the relative stability of the footwall. We infer that this deformation resulted from both the flexuring (Fig. 10) and the partitioning (Fig. 13b) processes.

This partitioning should not be considered exceptional. A similar phenomenon was described in the southern Longitudinal Valley of eastern Taiwan (Lee et al., 1998), where active oblique slip and fault creep occur (Angelier et al., 2000). It was interpreted in terms of stress-slip distribution, based on three-dimensional distinct element modelling (Hu et al., 2001). This similarity between the Longitudinal Valley Fault and the Chelungpu Fault is not surprising in light of their common behaviour as the two belt-parallel active boundaries of Taiwan (Angelier et al., 2001), where west-verging thrusting and left-lateral slip coexist.

6.7. Significance of the studied site with respect to regional fault slip

The Kuangfu school is located on the northern side of a valley, in an area where the fault strikes NW–SE, oblique at about 45° to the usual N–S trend of the Chelungpu Fault. Although the bend of the rupture trace is too small to be observable in regional maps (Fig. 1c), it was followed in the field and mapped at the 1:25,000 scale by the Central Geological Survey (1999a). With such an anomalous trend, the fault structure and slip may reflect local conditions rather than the regionally typical behaviour of the earthquake fault. At a place where the fault strikes N–S, near Wufeng (Fig. 11), we determined a near-surface dip angle of 30° (Angelier

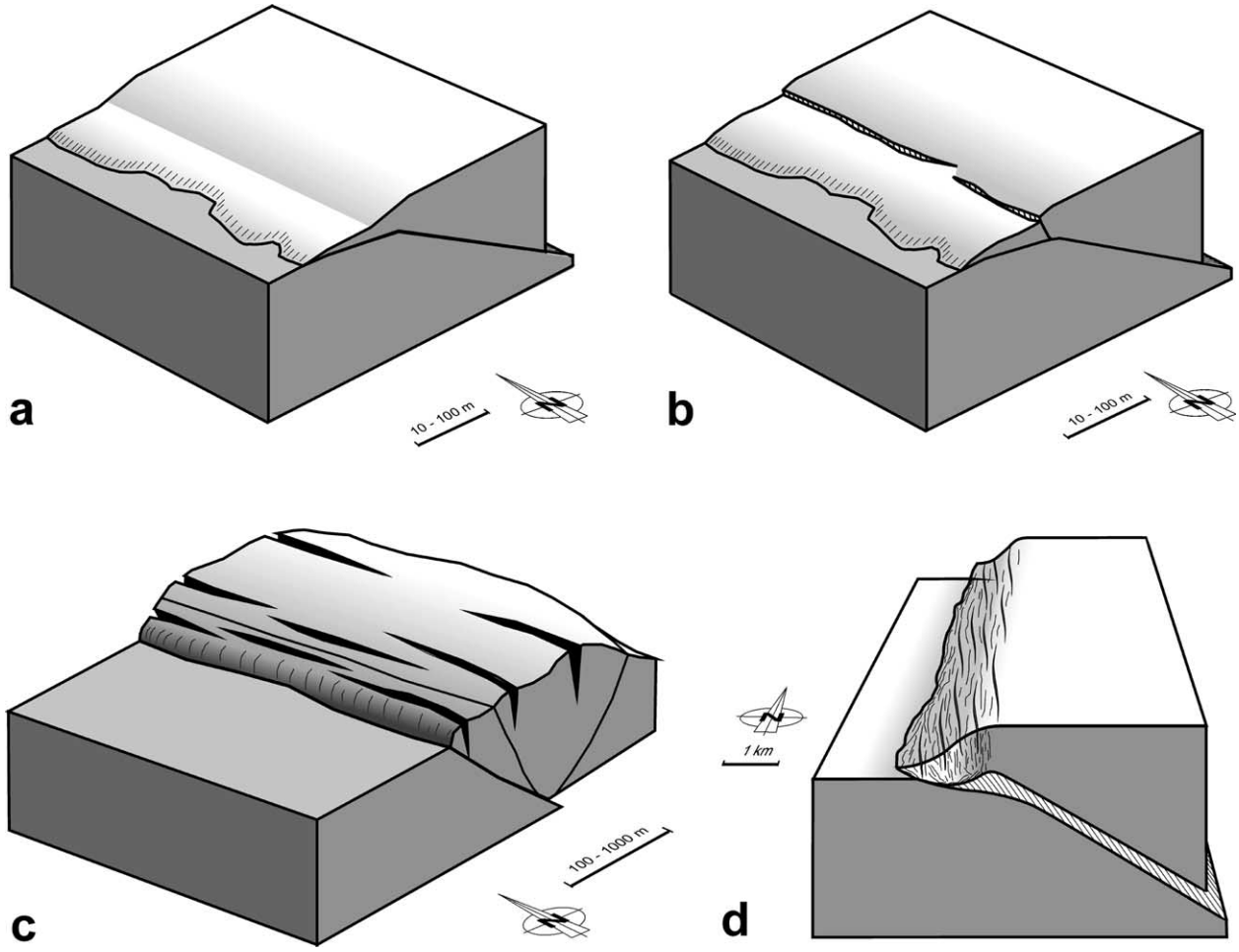

Fig. 14. Examples of near-surface variations in the dip-angle of a reverse fault. (a) Near-surface flattening of reverse fault and hanging wall flexure (see also Fig. 10b). (b) Steeply dipping reverse fault and low-relief thrust front above an upward-flattening reverse fault. (c) Pop-up structure, with thrust, backthrust and outward-fissured anticline above a reverse fault with upward-increasing dip angle. (d) Oblique-slip-related partitioning with dip-slip thrusting at thrust front and distributed left-lateral shear in hanging wall. At many places along the rupture trace of the September 21st, 1999, earthquake, (a), (b) or (c) are associated with (d).

et al., 2002). We also determined the three major displacement vectors (as defined in Fig. 13a): they were nearly the same as in Kuangfu, in terms of both the trends and the amplitudes. This suggests homogeneous kinematic behaviour despite the presence of the local fault bend in Kuangfu. At both localities, left-lateral shear along the N–S direction was accommodated in the hanging wall, east of the main rupture trace. The regional distribution of displacement vectors along the fault zone (Fig. 11) brings confirmation that partitioning is an usual feature rather than a local curiosity along the Chelungpu Fault.

In detail, the slip vectors trend 279° at Wufeng and 255° at Kuangfu, where the rupture trace respectively strikes N8°E and N141°E. The 47° change in fault strike induces a 24° variation in slip trend, both anticlockwise. The displacement vector trends oblique to fault strike at angles of 84° and 66° (left-lateral) in the two sites, respectively. This comparison shows that the rupture trace tends to behave as a dip-slip thrust, even where fault strike variations would require a large strike-slip component of motion according to a rigid body hypothesis. As obliquity increases, more and more differential deformation is accommodated by lateral shear in the hanging wall. The displacement in Kuangfu simply reveals amplified partitioning, as compared with the N–S trending segments of the Chelungpu Fault.

6.8. Relationship between fault attitudes at the surface and at depth

The co-seismic surface faults at the front of the Chelungpu thrust display a variety of attitudes (Fig. 14). In outcrops, the identification of a near-surface fault with the same attitude as the deeper thrust remains exceptional: this was the case near Wufeng, as mentioned above. A common feature is the near-surface flattening of the fault, which may result in deformation and tilting near the edge of the upthrust block (Fig. 14a). Also common is the presence of a steep-dipping reverse fault, which may result from two types of near-surface variation in fault dip. The first type occurs where the thrust reaches the surface at a very small

angle. The edge of the upthrust block may be broken by a reverse fault that accommodates large vertical motion, whereas most of the horizontal shortening occurs across the less visible thrust front (Fig. 14a). More of the observer's attention is usually paid to the high scarp than to the low relief thrust front. Because the steep reverse fault is believed to be the main expression of the thrust, the dip of the underlying fault is overestimated and the horizontal shortening is underestimated. A second type of relatively steep fault surface is found where the dip of the main fault increases upwards so that the thrust reaches the surface at a relatively high angle, inducing severe contraction in the shallow layers. In this case, pop-up structures commonly develop, with a backthrust in the upthrust block and an anticline affected by bending-related fissuring (Fig. 14c). The obliquity of thrust motion and the resulting partitioning in the hanging wall of the Chelungpu Fault induce further complexity (Fig. 14d).

The above examples highlight some simple sources of errors that may affect the determination of reverse fault attitude along a surface rupture trace. Common consequences of such errors, in the case of a reverse fault, are (1) the extrapolation at depth of steep fault dip angles observed at the surface and (2) accordingly, the underestimation of the horizontal shortening across the fault trace. Where no subsurface information is available, the most reliable indication about the actual dip of the reverse fault at shallow depths (approximately between 50 and 500 m) does not come from direct dip measurements on visible faults. This dip angle is obtained through a meticulous determination of the vertical offset, V, and the horizontal transverse offset, T (Fig. 6), across the fault zone (Fig. 9c). Such determination must take into account all contributions to deformation, not only in the surface rupture trace but also on its deformed edge zones (Fig. 5). The tangent of the dip angle, d, of the underlying fault is the ratio between these vertical and horizontal components of relative displacement in the vertical plane perpendicular to fault strike:

$$tgd = V/T \tag{16}$$

How the lateral component (L in Fig. 6), is determined, in order to reconstruct the three-dimensional fault displacement, has been thoroughly discussed in this paper. It is in any case essential to pay special attention to the complete geometrical reconstitution of the local deformation, the main purpose of this paper.

Acknowledgements

The co-operation between the French Institute in Taipei and the National Council of Taiwan, the authors' institutes and the Institut Universitaire de France supported the research work along the rupture trace of the September 1999 earthquake. The senior author thanks Dr H.E. Kuo Wei-Fan, Director of the BRT in Paris, for his help in the first days following the earthquake, and Dr J.P. Evans for constructive suggestions concerning the manuscript.

References

Angelier, J., 1986. Geodynamics of Eurasia–Philippine Sea Plate boundary: preface. Tectonophysics 125, IX–X.

Angelier, J., Bergerat, F., 2001. Behaviour of a rupture of the June 21st 2000, earthquake in South Iceland as revealed in an asphalted car park. Journal of Structural Geology in press (PII: S0191-8141(02)00007-X).

Angelier, J., Chu, H.-T., Lee, J.-C., Hu, J.-C., 2000. Active faulting and earthquake risk: the Chihshang Fault case, Taiwan. Journal of Geodynamics 29, 151–185.

Angelier, J., Lee, J.-C., Chu, H.-T., Hu, J.-C., Lu, C.-Y., Chan, Y.-C., Lin, T.-J., Font, Y., Deffontaines, B., Tsai, Y.-B., 2001. Le séisme de Chichi (1999) et sa place dans l'orogène de Taiwan. Comptes Rendus de l'Académie des Sciences Paris II 333 (1), 5–21.

Angelier, J., Lee, J.-C., Chu, H.-T., Hu, J.-C., 2002. Reconstruction of fault slip of the September 21st, 1999, Taiwan earthquake in the asphalted surface of a car park. Journal of Structural Geology in press (PII: S0191-8141(02)00038-X).

Central Geological Survey, 1999a. Surface ruptures along the Chelungpu fault during the Chi-Chi earthquake, Taiwan. Map at scale 1:25,000, Ministry of Economic Affairs, Republic of China, Taipei, 4 sheets.

Central Geological Survey, 1999b. Report of the geological survey of the 1999 Chi-Chi earthquake (in Chinese). Central Geological Survey, MOEA, Taipei.

Central Weather Bureau of Taiwan, 1999. The Chi-Chi Earthquake in Taiwan. Internet site at address http://www.cwb.gov.tw.

Chinese Petroleum Corporation, 1974. Geological map of Miaoli, scale 1:100,000. Chinese Petroleum Corporation, Taiwan.

Chinese Petroleum Corporation, 1982. Geological map of Taichung, scale 1:100,000, Chinese Petroleum Corporation, Taiwan.

Chung, J.-K., Shin, T.-C., 1999. Implication of the rupture process from the displacement distribution of strong ground motions recorded during the 21 September 1999 Chi-Chi, Taiwan earthquake. Terrestrial Atmospheric Ocean, Taipei 10, 777–786.

Ho, C.-S., 1975. An introduction to the geology of Taiwan: explanatory text of the geologic map of Taiwan. Ministry of Economic Affairs, Republic of China, Taipei, 153pp.

Ho, C.-S., 1986. A synthesis of the geologic evolution of Taiwan. Tectonophysics 125, 1–16.

Hou, C.-S., Lai, T.-C., Fei, L.-Y., Wang, J.-S., Chen, W.-H., 2000. Highly accurate surveying in the study of the Chelungpu active fault-comparison of the data before and after the Chi-Chi Earthquake. Central Geological Survey (MOEA, Taipei) Special Publication 12, 191–210.

Hu, J.-C., Angelier, J., Homberg, C., Lee, J.-C., Chu, H.-T., 2001. Three-dimensional modeling of the behavior of the oblique convergent boundary of southeast Taiwan: friction and strain partitioning. Tectonophysics 333, 261–276.

Institute of Earth Sciences, Academia Sinica, 1999. The Chi-Chi Earthquake in Taiwan. Internet site at address http://www.earth.sinica.edu.tw/921/921chichi_main_eng.htm.

Johnson, K., Hsu, Y.J., Segall, P., Yu, S.B., 2001. Fault geometry and slip distribution of the 1999 Chi-Chi, Taiwan earthquake imaged from inversion of GPS data. Geophysical Research Letters 28, 2285–2288.

Kao, H., Chen, W.-P., 2000. The Chi-Chi earthquake sequence: active out-of-sequence thrust faulting in Taiwan. Science 288, 2346–2349.

Kao, H., Angelier, J., 2001a. Stress tensor inversion for the Chi-Chi earthquake sequence and its implications on regional collision. Bulletin of the Seismological Society of America 91 (5), 1028–1040.

Kao, H., Angelier, J., 2001b. The Chi-Chi Earthquake sequence, Taiwan: results from source parameters and stress tensor inversions. Comptes Rendus de l'Académie des Sciences Paris II 333 (1), 65–80.

Lee, J.-C., Angelier, J., Chu, H.-T., Yu, S.-B., Hu, J.-C., 1998. Plate-boundary strain partitioning along the sinistral collision suture of the Philippine and Eurasian plates: analysis of geodetic data and geological observation. Tectonics 17 (6), 859–871.

Lee, J.-C., Chu, H.-T., Angelier, J., Chan, Y.-C., Hu, J.-C., Lu, C.-Y., Rau, R.-J., 2001. Geometry and structure of northern surface ruptures of the 1999 Mw = 7.6 Chi-Chi, Taiwan earthquake: influence from inherited fold belt structures. Journal of Structural Geology 24 (1), 173–192.

Lin, A., Ouchi, T., Chen, A., Maruyama, T., 2001. Co-seismic displacements, folding and shortening structures along the Chelungpu surface rupture zone occurred during the 1999 Chi-Chi (Taiwan) earthquake. Tectonophysics 330, 225–244.

Ma, K.-F., Lee, C.-T., Tsai, Y.-B., Shin, T.-C., Mori, J., 1999. The Chi-Chi, Taiwan earthquake: large surface displacements on an inland thrust fault. EOS Transactions 80, 605–611.

Mouthereau, F., Angelier, J., Lee, J.-C., 2001a. Interprétation structurale du séisme du 21 septembre 1999 au front de la chaîne de Taiwan: "thin-skin" ou "thick-skin"? Comptes Rendus de l'Académie des Sciences Paris II 333 (1), 93–103.

Mouthereau, F., Lacombe, O., Deffontaines, B., Angelier, J., Brusset, S., 2001b. Deformation history of the southwestern Taiwan foreland thrust belt: insights from balanced cross-sections and syntectonic deposits analysis. Tectonophysics 333, 293–322.

Roberts, D., 2000. Pull-apart stepover structures in an asphalted road surface—a geological curiosity. Journal of Structural Geology 22, 1469–1472.

Suppe, J., 1976. Decollement folding in southwestern Taiwan. Petroleum Geology of Taiwan 13, 25–35.

Suppe, J., 1981. Mechanics of mountain building in Taiwan. Memoirs of the Geological Society of China 4, 67–89.

Tsai, Y.-B., 1986. Seismotectonics of Taiwan. Tectonophysics 125, 17–38.

Wu, F.T., 1978. Recent tectonics of Taiwan. Journal Physics Earth 26 (suppl.), S265–S299.

Yu, S.-B., Chen, H.-Y., Kuo, L.-C., 1997. Velocity field of GPS stations in the Taiwan area. Tectonophysics 274, 41–59.

Yu, S.-B., Kuo, L.-C., Hsu, Y.-J., Su, H.-H., Liu, C.-C., Hou, C.-S., Lee, J.-F., Lai, T.-C., Liu, C.-C., Liu, C.-L., Tseng, T.-F., Tsai, C.-S., Shin, T.-C., 2001. Preseismic deformation and coseismic displacements associated with the 1999 Chi-Chi, Taiwan, earthquake. Bulletin of the Seismological Society of America 91 (5), 995–1012.